Scanning drift tube measurements and kinetic studies of electron transport in CO

S Dujko[1],[*] , **D Bošnjaković[1]** , **M Vass[2,3]** , **P Hartmann[2]** , **I Korolov[3]** , **N R Pinhão[4]** , **D Loffhagen[5]** and **Z Donkó[2]**

[1] Institute of Physics Belgrade, University of Belgrade, Pregrevica 118, 11080 Belgrade, Serbia
[2] Institute for Solid State Physics and Optics, Wigner Research Centre for Physics, Konkoly-Thege Miklós Str. 29-33, 1121 Budapest, Hungary
[3] Chair of Applied Electrodynamics and Plasma Technology, Department of Electrical Engineering and Information Science, Ruhr-University Bochum, 44780 Bochum, Germany
[4] Instituto de Plasmas e Fusão Nuclear, Instituto Superior Técnico, Universidade de Lisboa, Av. Rovisco Pais, 1049-001 Lisboa, Portugal
[5] Leibniz Institute for Plasma Science and Technology, Felix-Hausdorff-Str. 2, 17489 Greifswald, Germany

E-mail: sasha@ipb.ac.rs

CrossMark

Abstract

We present scanning drift tube measurements of electron swarm transport coefficients in CO as a function of the reduced electric field E/N at room temperature under time-of-flight conditions. The measurements are compared to modeling results and other available experimental data on swarm transport over the broad range of E/N from 2 Td to 1603 Td. The modeling results are obtained in Monte Carlo simulations and by solving the electron Boltzmann equation using a multi-term approach and the density gradient expansion procedure. We find generally good agreement between the measured and calculated transport coefficients. We propose a strategy to improve the cross-section set used to explain certain discrepancies at lower E/N values. Measurements and calculations of electron transport coefficients under hydrodynamic conditions are complemented by Monte Carlo simulations of electron transport in an idealized steady-state Townsend (SST) setup. The ionization coefficient is calculated as a function of E/N from the spatial density profiles of the electrons and compared to the corresponding values evaluated from the knowledge of the effective ionization frequency, drift velocity and longitudinal diffusion coefficient. Contrary to the traditional views, according to which the spatial relaxation of the mean energy and other transport properties for electrons in molecular gases is most commonly monotonic or quasi-monotonic, we find a 'window' of E/N where the SST transport properties of the electrons exhibit oscillatory behavior as they relax towards the equilibrium state far downstream from the electron emitting boundary.

Keywords: electron swarm transport coefficients, drift tube measurements, Boltzmann equation, Monte Carlo simulation, kinetic theory and computations

(Some figures may appear in colour only in the online journal)

---

[*] Author to whom any correspondence should be addressed.

1. Introduction

The knowledge of electron collisions and transport processes in CO is of key importance for understanding fundamental electron–CO interactions that occur in nature and in a wide variety of technological applications. CO is one of the main constituent molecules of Martian and Venusian upper atmospheres [1, 2] and it most likely had played a significant role in the prebiotic chemistry and synthesis of organic molecules in the weakly reducing atmosphere of Primordial Earth [3]. Electron collisions with the CO molecule are also important for observing and modeling infrared CO emissions from Jupiter, Uranus, Neptune and Titan (see [2] and references therein). In particular, the presence of CO in Titan's atmosphere reduces the production of tholins [4] and strongly affects both number density and particle size of the aerosols [5]. Similar effects have recently been examined in the atmosphere of Triton, Neptune's largest satellite [6]. Electron scattering by CO is also relevant for studies of cometary [7, 8] and exoplanet atmospheres [9, 10]. Furthermore, since CO is one of the most abundant gases in the molecular clouds of the interstellar medium, studies of electron–CO interactions are important in astrochemistry [11, 12].

CO also has a broad range of plasma-based technology applications, ranging from plasma etching [13, 14] and plasma medicine [15] to gas lasers [16–20] and *syngas*[6] production [21–23]. In particular, CO is an unavoidable component of CO_2-containing plasmas, as both of these molecular species are involved in a number of common chemical reactions [24]. Recent experimental and modeling studies on the production of oxygen on Mars are a good example in this context [25, 26]. Another example is the activation of the CO_2 molecule using a wide range of plasma sources, where the CO molecule is one of the most important resultant species [27, 28]. The further development of these technologies depends on an accurate knowledge of the cross sections for electron scattering with CO, the transport properties, and the electron-induced processes involved.

In the literature, some cross-section sets for electron scattering with CO were already reported. Experimental work on electron collisions in CO prior to the mid-1980s is summarized in the review article of Trajmar *et al* [29]. More recently, cross sections for electron–CO interactions were reviewed by Itikawa and a recommended cross-section set was produced [12]. Similar work was performed by Brunger and Buckman [30], and Anzai *et al* [31]. As noticed by Vialetto *et al* [32], these cross-section sets are not complete and cannot be directly used as input data in kinetic modeling of electron swarms and plasmas. The first complete cross-section sets for electron scattering in CO were developed by Hake and Phelps [33], and Land [34]. The former is tabulated and is available in the Phelps database of LxCat [35]. Poparić *et al* studied vibrational excitation of the CO molecule experimentally [36], and subsequently a complete set of cross sections was

formed incorporating other relevant processes. Using these cross sections as input in Monte Carlo simulations, rate coefficients for electron impact excitation in DC [37] and RF [24] electric fields as well as ionization rate coefficients in RF electric fields [38] were calculated.

Quite recently, complete cross-section sets were developed by Biagi [39] and the Lisbon group [40]. Among many important points, the swarm-derived cross-section set of the Lisbon group was developed with the particular focus on the correct implementation of rotational excitation and de-excitation processes for calculating the electron swarm transport coefficients at lower values of E/N. The cross-section set can be found in the IST-Lisbon database [41] within LxCat. The accuracy of the proposed cross-section set was tested using the Lisbon KInetics two-term Boltzmann solver [42]. The calculated electron swarm transport properties were compared with experimental measurements at different gas temperatures and fairly good agreement was found. A further refinement of this cross-section set was performed by Vialetto *et al* [32] by considering different angular scattering models for rotational collisions in Monte Carlo simulations and two-term Boltzmann equation (BE) based studies. As a result of this study, a novel anisotropic scattering model was derived from the dipole-Born differential cross sections, describing the strongly forward-peaked nature of rotational collisions. In the same study, the electron impact cross sections from Biagi's Magboltz code v11.10 [39] were also considered.

The present paper contributes to this body of work by performing measurements of the electron swarm transport coefficients in CO using the scanning drift tube technique [43]. This technique has previously been used to measure the electron swarm transport coefficients in a variety of atomic and molecular gases [44–47] and to investigate the spatially and temporally resolved electron kinetics in a homogeneous electric field in argon gas, in the vicinity of an emitting boundary [48].

The additional important aspect of the present work is that we use the most recent cross-section set of electron scattering with CO, which was developed and tabulated by Biagi in Magboltz v11.11 [39]. This set of cross sections was used as input in simulations of the electron's motion in our experimental system and kinetic calculations using a multi-term approach and the density gradient expansion procedure for the solution of the electron BE. Among many important points, the new and updated cross-section set offers a possibility to include the anisotropic scattering for dipole rotational collisions, which is based on the angular scattering model initially proposed by Okhrimovskyy *et al* [49]. As our measurements were carried out over the E/N range where the effects of rotational excitations are minimal, we applied the isotropic model of scattering for both dipole and quadrupole rotational excitations.

In this paper, as part of our ongoing investigations of electron transport in CO, we also study the spatial relaxation of electrons in an idealized steady-state Townsend (SST) setup using a Monte Carlo simulation technique. The generalization of hydrodynamic conditions to non-hydrodynamic conditions allows a better understanding of the electron transport near the emitting electrode and the exact calculation of the effective

---

[6] *Syngas* or synthesis gas is a mixture of H_2 and CO used as raw material in several chemical processes.

SST ionization coefficient. In studies on the spatial relaxation of electrons under SST conditions using Monte Carlo and/or BE results, the primary focus has usually been on electrons in atomic gases [50–63]. Some results related to N_2 [52, 64], CF_4 [56], CO_2 [59], CH_4 [65] and synthetic air [66] can also be found in the literature.

The primary purpose of this work is: (i) to present the scanning drift tube measurements of electron swarm transport coefficients and make comparisons with previous measurements, (ii) to test the completeness and consistency of the most recent Biagi's cross-section set for electron scattering in CO by comparing the measured electron swarm transport coefficients with those obtained from kinetic calculations and simulations, and (iii) to investigate the spatial relaxation of electrons in an idealized SST setup in CO with the particular emphasis upon the calculation of the reduced effective Townsend ionization coefficient. The remainder of this paper is organized as follows. In section 2, we briefly review the scanning drift apparatus for the measurement of electron swarm transport coefficients. In section 3, we outline the most recent cross-section set for electron scattering in CO from Magboltz v11.11, including the treatment of superelastic collisions. In section 4, we present the methods of our calculations, including the basic elements of a multi-term approach and density gradient expansion procedure for solving the electron BE. We also discuss the Monte Carlo method for simulating the electron swarm transport properties in an infinite volume under hydrodynamic conditions and under non-hydrodynamic conditions in an idealized SST setup. The results of this work are then given in section 5. We begin with a brief outlook of the previous measurements of electron swarm transport properties in CO. After discussing the electron distribution function for time-of-flight (TOF) and SST conditions, the experimentally measured drift velocity, longitudinal diffusion coefficient and effective ionization coefficient are presented in section 5.3, along with a comparison of calculations using the electron impact cross sections from Magboltz v11.11. In section 5.4 we present the results of our study under non-hydrodynamic conditions in an idealized SST setup. Finally, in section 6 we draw some conclusions from the present study.

2. Experimental system

Our measurements of the electron transport coefficients are conducted with a 'scanning' drift tube apparatus [43], which has already been used for measurements in a number of gases such as argon, synthetic air, methane, deuterium, carbon dioxide as well as in acetylene, ethylene, and ethane [44–47]. These previous publications provide a detailed description of the experimental system. Therefore, only its main features are presented here. The system operates under TOF conditions: a cloud of electrons is initiated at $t = 0$ and its progression is traced by detecting particles beyond a drift region whose length is varied. The simplified scheme of the experimental apparatus is shown in figure 1.

The drift cell is situated within a stainless steel vacuum chamber, which can be evacuated by a turbomolecular pump
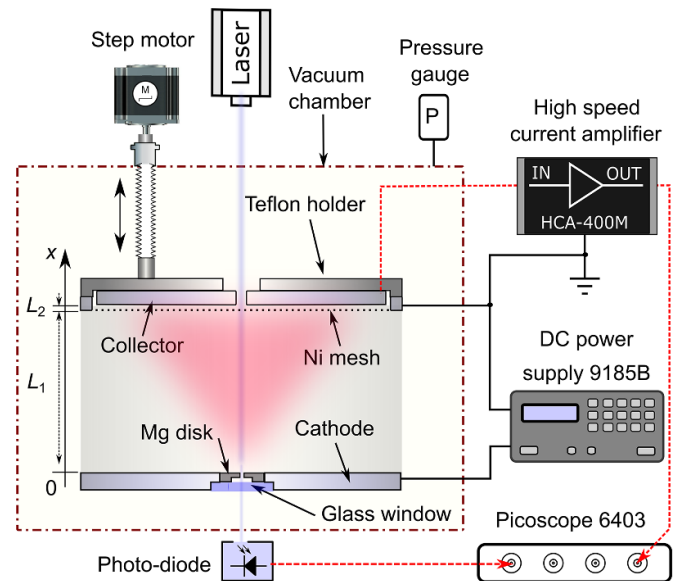

Figure 1. Simplified schematic of the scanning drift tube apparatus.

backed with a rotary pump, to a base pressure of the order of $\sim 10^{-7}$ mbar. Carbon monoxide is supplied from a Linde Minican container into the chamber via a mass flow controller and its pressure is monitored with a Pfeiffer CMR 362 capacitive gauge.

Electron swarms are initiated with $\approx 1.7\,\mu$J UV (266 nm) light pulses of a frequency-quadrupled diode-pumped YAG laser. The light of the laser enters the vacuum chamber via a feedthrough equipped with a quartz window. Mg is used as emitter material at the center of the negatively biased (cathode) electrode.

The drift cell consists of two regions, which are separated by a fine Ni mesh (with $T = 88\%$ 'geometric' transmission and 45 lines/inch density):

- Region (i) is the *cathode-mesh region* with a length of L_1, which is variable and can be set by a step motor via a vacuum feedthrough. In this region, a homogeneous electric field is established by biasing the cathode to a negative potential that is provided by a BK Precision 9185B power supply. The mesh is electrically grounded. When the drift length L_1 is changed, the cathode-mesh potential difference is adjusted to ensure a fixed E/N irrespective of L_1. During the scan we use 53 values of the drift length, L_1 is varied between 7.8 mm and 58.3 mm.

- Region (ii) is the *mesh-collector region*, which the electrons enter from region (i) via the openings of the mesh. The collector is a flat stainless steel electrode positioned at a fixed distance of $L_2 = 1$ mm behind the mesh. This electrode is connected to a high speed current amplifier (type Femto HCA-400M) that has virtually grounded input. The amplified signal is recorded by a digital oscilloscope (type Picoscope 6403B) with sub-ns time resolution. In this region of the cell there is no electric field. The measured signal is generated by the moving charges within the mesh-collector gap: according to the Shockley–Ramo theorem [67–69] the
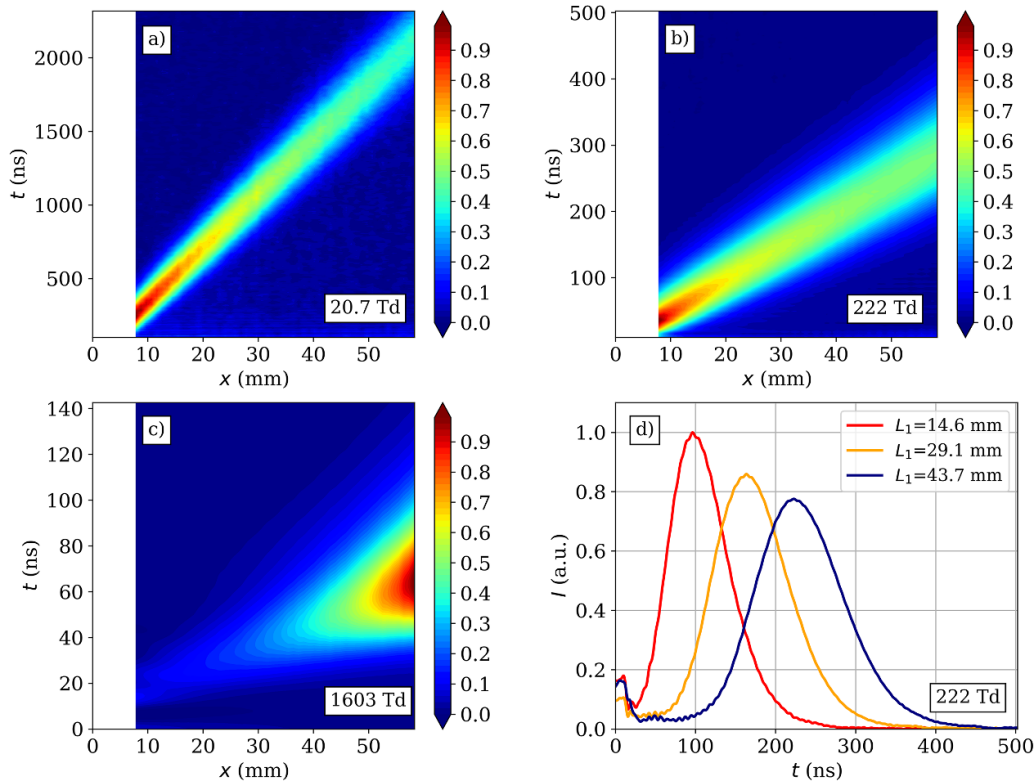
Figure 2. Measured swarm maps for different values of E/N in CO (a)–(c), and vertical cuts of panel (b), which are the measured current traces at the respective gap distances given in the legend (d). The data (for the measured current) shown in panels (a)–(c) have been normalized to a maximum of 1.0.

current induced by an electron moving in a gap between two plane-parallel electrodes with a velocity v_x perpendicular to the electrodes is $I = -e_0 v_x/L$, where $-e_0$ is the charge of the electron and L is the distance between the electrodes ($L = L_2$ in our case). The measured current at a given time t is

$$I(t) = c \sum_k v_{x,k}(t), \qquad (1)$$

where c is a constant. The summation goes over all electrons which are present in Region (ii) at time t, and $v_{x,k}$ is the velocity component of the kth electron in the x direction.

In panels (a)–(c) of figure 2 we illustrate some of the measured 'swarm maps' which represent the raw experimental results. These maps are composed from current traces recorded at 53 different values of the drift length (L_1). A few of these traces are shown in figure 2(d) for three values of L_1, for the case of $E/N = 222\,\text{Td}$. The swarm map obtained at 20.7 Td shows a straight line whose width increases only slightly with the space coordinate x, corresponding to a low rate of (longitudinal) diffusion. The inverse of the slope of the line corresponds to the bulk drift velocity. With increasing E/N, the onset of ionization can also be observed. This becomes quite significant at $E/N = 1603\,\text{Td}$ as revealed by the rapidly growing magnitude of the measured current with the position.

The derivation of the electron swarm transport coefficients includes the bulk drift velocity, the bulk longitudinal diffusion coefficient and the ionization frequency. It is based on the fitting of the swarm maps using the solution of the diffusion equation under hydrodynamic conditions [70, 71]. As shown in our previous work [46], this procedure has an acceptable accuracy. However, the peculiarities of the detector system used in the drift tube call for adjustments of the measured transport characteristics as explained below.

Electrons entering Region (ii) (the gap between the mesh and the collector) contribute to the measured current until their first collisions with the background gas molecules, as these collisions randomize their velocities. The free path of the electrons, for this reason, plays a crucial role in the magnitude of the current. If the free path is longer than L_2, the electron reflection/sticking property of the collector material plays an important role too, as the reflected electrons generate a current contribution with an opposite sign with respect to that generated by the 'incoming' electrons. These effects have been analyzed in detail in [48]. It was found that the sensitivity of the detector system changes with the pressure and the energy distribution of the electrons (and it depends of the gas itself, too).

Because of these dependencies, a correction procedure was developed [46], which is based on the simulation of the electron's motion in the experimental system, under the same conditions at which experimental recordings for the transport coefficients are made. These simulations also create a set of swarm maps, which are also fitted by the same functional

form as the experimental swarm maps. At the same time, zero-dimensional kinetic calculations are also carried out using the same cross section set as in the simulations of the experimental system and the resulting transport coefficients are compared with those obtained from the fitting of the maps originating from the simulations. The deviations observed here originate from the imperfections of the measurement and data acquisition methods and can be used to correct the transport coefficients obtained from the experiments. For more details see [46].

3. Cross sections for electron scattering in CO

In this work, we use the most recent cross-section set of electron scattering in CO, initially released by Biagi in Magboltz v11.11 []. The cross-section set is stored internally and coded directly into Magboltz v11.11, a publicly accessible Monte Carlo code for calculating electron swarm transport coefficients. The cross-section set is developed on the basis of a previous assessment of electron–CO collision cross sections in Magboltz v11.10 [39] extended by recent measurements of cross sections for vibrational excitations of the ground vibrational state [72] and anisotropic scattering for the dipole rotational collisions based on the angular scattering model by Okhrimovskyy *et al* [49]. Additional new elements include measured oscillator strengths for dipole transitions and cross sections for a number of dissociative ionizations. In order to improve the consistency of the cross-section set with the experimental swarm data, the measurements of drift velocity and diffusion coefficients normalized to mobility by Haddad and Milloy [73], Petrović and Crompton [74], Nakamura [75], Saelee and Lucas [76] and Pack *et al* [77] were used in the swarm analysis.

The new and updated cross-section set from Magboltz v11.11 was not modified during the calculations in the present work. In other words, no iterative process was used to modify the cross sections to improve agreement between the calculated transport coefficients and those from previous and current measurements. However, the most recent set of cross sections, which has been extracted from Magboltz v11.11 and used here for calculations, differs considerably from the cross-section set in Magboltz v11.10. This difference suggests the need to test the coherence between the latest version of the Magboltz v11.11 cross sections and our combined measurements and calculations. For clarity and better visibility, the cross sections used here are displayed in panels (a)–(c) in figure 3.

The elastic momentum transfer cross section and cross sections for rotational excitations are shown in figure 3(a). Cross sections for rotational excitations were calculated using the Born approximation for the dipole rotation interaction. The total number of rotational transitions is 55, where 28 cross sections are the transitions from the kth to the $k+1$ level, i.e. dipole rotational states. The remaining 27 cross sections refer to the transitions from the kth to the $k+2$ level, where
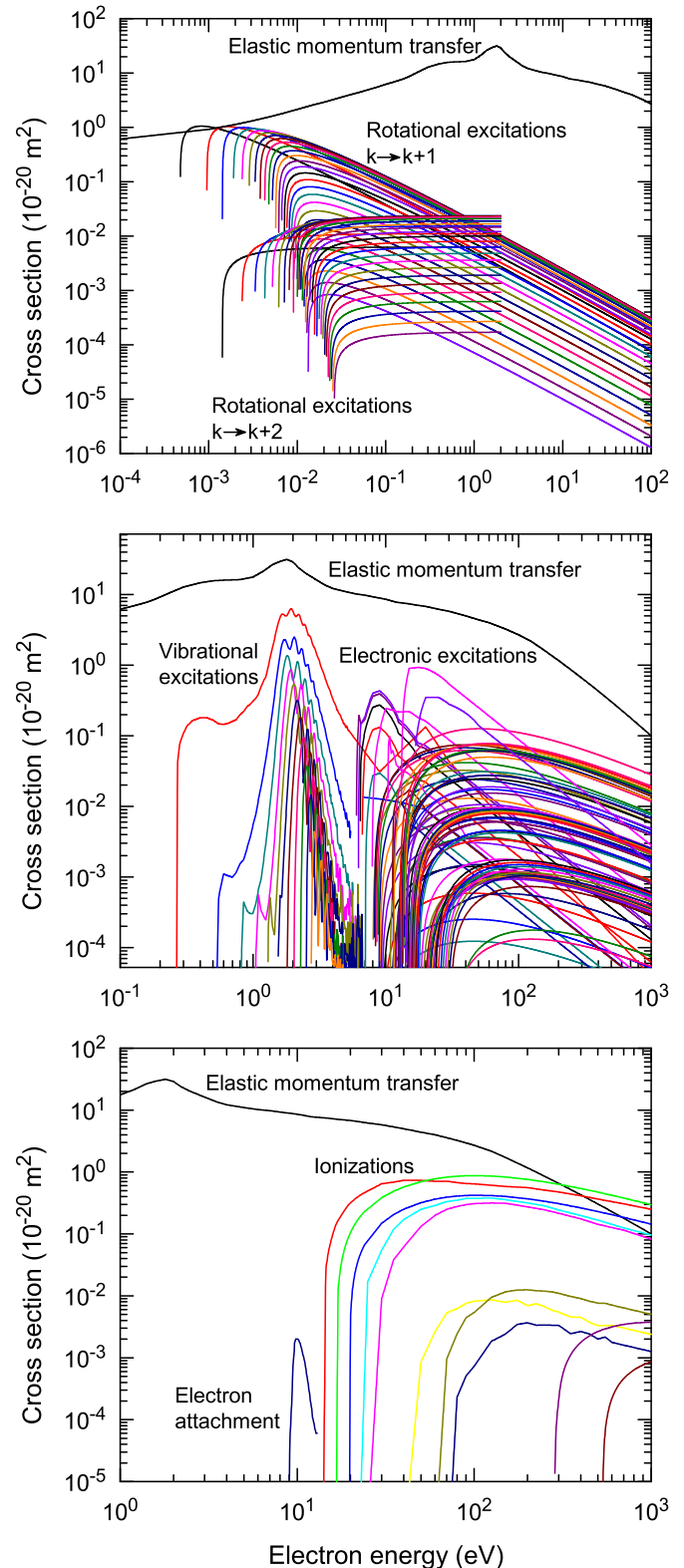

Figure 3. Cross sections for electron scattering in CO: (a) cross sections for elastic momentum transfer and rotational excitations. The rotational cross sections are multiplied by the corresponding rotational level population at 293 K, (b) cross sections for vibrational excitations, electronic excitations, dissociation into neutral fragments and dissociation of the Rydberg states, and (c) cross sections for electron-impact ionization and dissociative attachment.

the rotational levels are calculated based on the electric quadrupole moment of the CO molecule. As can be seen from the figure, the cross sections for dipole rotational transitions are extrapolated to high energies, while the cross sections for quadrupole rotational transitions are simply reduced to zero values for electron energies greater than approximately 2 eV.

Figure 3(b) shows cross sections for vibrational excitation, electronic excitation, and dissociation into neutral fragments. For comparison, the elastic momentum transfer cross section is also shown. The present set includes 11 cross sections for vibrational excitations. The cross sections were obtained by integrating experimentally determined differential cross sections for vibrational excitations over a wide range of scattering angles and electron energies [72]. As for the electronic excitation, the angle-integrated cross sections for vibrational excitation $v' = 0, 1, \ldots, 5$–10 of the triplet state $A^3\Pi$, vibrational excitations $v' = 0, 1, \ldots, 12$ of the singlet state $A^1\Pi$ and vibrational excitations $v' = 0, 1$ of the singlet states $B^1\Sigma$, $C^1\Sigma$ and $E^1\Pi$, respectively, are included in the present set. In addition to the cross sections for vibrational excitation of electronic states, this set contains cross sections for the excitations of the singlet states $B^1\Sigma$, $C^1\Sigma$, $F^1\Sigma$, $J^1\Sigma$ and $L^1\Pi$, as well as the cross sections for the excitations of the triplet states $a'^3\Sigma$, $B^3\Sigma$, $J^3\Sigma$ and $C^3\Pi$. Electronic excitations for singlet states $E^1\Pi$, $F^1\Sigma$, $J^1\Sigma$ and $L^1\Pi$ are dissociative. Furthermore, the current set of cross sections includes cross sections for the dissociation of Rydberg states, the sum of triplet states, and cross sections for neutral dissociation whose energy thresholds are greater than the threshold of the cross section for electron impact ionization of CO molecules in the ground state.

Figure 3(c) displays the cross sections for ionization and dissociative electron attachment. For comparison, the cross section for transfer of momentum in elastic collisions is also displayed. The total cross section for ionization is divided into different channels, with different final products. The cross section with the lowest threshold of 14.014 eV describes the electron impact ionization of a CO molecule in the ground state resulting in a CO^+ ion. The remaining cross sections describe dissociative ionizations whose products are CO^+ ions in the electronic excited states $A^2\Pi$, $B^2\Sigma$, respectively, the cross sections for the production of C^+ and O^+ ions and cross sections for the production of doubly ionized C^{++}, and O^{++} ions. The last two cross sections describe ionization from the K-shell of atomic carbon and oxygen, whose energy thresholds of 285 eV and 532 eV, respectively, are much higher than those for the production of CO^+ ions.

Dissociative electron attachment in a CO molecule may lead to the production of O^- or C^- negative ions. The cross section for the dissociative electron attachment used in this work is total and is not divided into individual cross sections for the production of O^- or C^- negative ions. As can be seen from figure 3(c), the cross section of dissociative electron attachment extends in a very narrow energy range, approximately between 9 eV and 11 eV, and then its value drops sharply. The maximal value is between 9.9 eV and 10 eV.

As for the cross sections for superelastic collisions, they were obtained on the basis of the principle of detailed balance and were calculated exclusively for cross sections for rotational excitation and the cross section for vibrational excitation with a threshold of 0.266 eV. This is justified if we take into account that the transport coefficients are calculated at room temperature, and the first following cross section for vibrational excitation has an energy threshold of 0.528 eV. In other words, the influence of superelastic collisions, which correspond to this vibrational excitation and the remaining inelastic collisions with higher threshold energies, is minimal on the distribution function and transport coefficients at a temperature of 293 K.

4. Methods of calculations

4.1. The diffusion equation: connecting the scanning drift tube apparatus and theory

The scanning drift tube apparatus may operate in the regime of strong gradients incorporating the non-hydrodynamic effects in the close vicinity of the emitting electrode and in a weak gradient regime, far away from the boundaries, where hydrodynamic conditions generally prevail [43, 48]. Transport coefficients of the electrons are constant in both space and time and they are exclusively defined in a weak gradient regime, under hydrodynamic conditions [71, 78]. This suggests that the present experimental setup should be directly analyzed via the diffusion equation

$$\partial_t n(\boldsymbol{r}, t) + \boldsymbol{W} \cdot \nabla n(\boldsymbol{r}, t) - \boldsymbol{D} : \nabla \nabla n(\boldsymbol{r}, t) = n(\boldsymbol{r}, t) \nu_{\text{eff}}, \quad (2)$$

where $n(\boldsymbol{r}, t)$ is the electron number density, $\nu_{\text{eff}} = \nu_i - \nu_a$, the effective ionization frequency is the difference of the ionization (ν_i) and attachment (ν_a) frequencies, $\boldsymbol{W}$ is the bulk drift velocity, and $\boldsymbol{D}$ is a bulk diffusion tensor with two independent components, the bulk longitudinal diffusion coefficient, D_L and the bulk transverse diffusion coefficient, D_T. The present experimental measurements were carried out under conditions where the effects induced by higher order transport coefficients are negligible, limiting the diffusion equation to drift and diffusion only [79, 80].

The present discussion can be further simplified for the scanning drift tube apparatus as the spatial gradients in the electron number density are present only along the electric field direction. As the electric field lies along the *x*-axis, then equation (2) reduces to

$$\partial_t n(x, t) + W \partial_x n(x, t) - D_L \partial_x^2 n(x, t) = n(x, t) \nu_{\text{eff}}. \quad (3)$$

Assuming the following initial and boundary conditions

$$n(x, 0) = n_0 \delta(x),$$
$$n(x, t) = 0, \ (x \to \infty, t > 0), \quad (4)$$

the solution of equation (3) is given by [70]:

$$n(x, t) = \frac{n_0}{(4\pi D_L t)^{1/2}} \exp\left[\nu_{\text{eff}} t - \frac{(x - Wt)^2}{4 D_L t}\right], \quad (5)$$

where n_0 is the initial electron density. This solution represents a Gaussian pulse, whose peak drifts with the bulk drift

velocity W and diffuses about the center-of-mass according to the bulk longitudinal diffusion coefficient, D_L. This expression describes the spatio-temporal evolution of the electron density and represents the direct connection between the scanning drift tube apparatus and theory. In the present work, this solution of the diffusion equation is fitted using the transport coefficients ν_{eff}, W and D_L as adjustable variables, until the best fit of the measured signal for each E/N is obtained. Based on the various sources of experimental uncertainties (e.g. the gap length, time resolution, the temporal stability of the laser intensity, noise level, etc) we estimate that the value of the reduced electric field is determined within 3% for E/N-values $\geqslant 8\,\text{Td}$, and this uncertainty increases up to 12% for values down to 2 Td. Similarly, the accuracy of the determined drift velocity is $\leqslant 3\%$, while for the longitudinal diffusion coefficient and the effective ionization coefficient, the data points with errors greater than 15% were not considered.

In addition to the bulk transport coefficients, flux transport coefficients may be defined using the flux gradient relation [78]. Expanding the flux of the electrons in terms of gradients of $n(x,t)$ assuming the one-dimensional (1D) case, we get

$$\Gamma(x,t) = W^{\star} n(x,t) - D_L^{\star} \partial_x n(x,t), \tag{6}$$

where $W^{\star}$ and $D_L^{\star}$ are the flux drift velocity and the flux longitudinal diffusion coefficient, respectively. Although the flux transport coefficients are not directly measurable quantities in swarm experiments, including the scanning drift tube apparatus, they play an important role in plasma modeling [81]. Both families of the transport coefficients, the bulk and the flux, are discussed for electrons in CO in the present study.

In the present work we extend the study of electron transport in CO under hydrodynamic conditions by considering the electrons under non-hydrodynamic conditions in an idealized SST setup. A stream of electrons emitted from one of the electrodes enters and ionizes the CO gas, and at a sufficiently large distance x, the equilibrium state forms [55, 65]. In this spatial region, it is usually assumed that the electron number density may be represented as

$$n(x) \sim n_0 \exp(\alpha_{eff} x), \tag{7}$$

where α_{eff} is the effective Townsend ionization coefficient. The approximate expression for the effective Townsend ionization coefficient may be derived by substituting equation (7) into equation (3) and assuming that gradients of the electron number density are small [82, 83]. The expression is given by

$$\alpha_{eff} = \frac{W}{2D_L} \pm \sqrt{\left(\frac{W}{2D_L}\right)^2 - \frac{\nu_{eff}}{D_L}}, \tag{8}$$

where ν_{eff}, W and D_L are hydrodynamic values of the effective ionization frequency, bulk drift velocity and bulk longitudinal diffusion coefficient, respectively. It is legitimate to omit the plus sign in equation (8) for an infinite gas while in the presence of the electrodes, both roots are required [84]. As we consider an idealized SST experiment, where the stream of electrons is produced by an emitting boundary in the half-space,

we apply the form of equation (8), in which the positive root is dismissed.

4.2. BE analysis

Different methods are applied to solve the BE

$$\partial_t f + \boldsymbol{v} \cdot \nabla_r f - \frac{e_0}{m} \boldsymbol{E} \cdot \nabla_v f = C(f) \tag{9}$$

for electron swarms in a background gas with density N and acted upon by a constant electric field, $\boldsymbol{E}$. Here, $f(\boldsymbol{r}, \boldsymbol{v}, t)$ is the electron velocity distribution function (EVDF), $\boldsymbol{r}$, $\boldsymbol{v}$ and t are the position, velocity and time, respectively, m denotes the electron mass and $C(f)$ is the linear collision operator. The numerical approaches include a multi-term method for the solution of equation (9) under spatially homogeneous and SST conditions, respectively, as well as the S_n method applied to a density gradient expansion of the EVDF. These methods differ in their initial physical assumptions and in the numerical algorithms used and provide different properties of the electron swarms. In all BE methods, however, we assume isotropic electron scattering in all inelastic collision processes and that the kinetic energy available after each ionization event is shared equally between the two electrons in accordance with [85].

Details of the different BE methods have been discussed in [45], and we just provide a brief discussion below.

In the present investigations, the electric field is parallel to the x-axis and points in negative direction, $\boldsymbol{E} = -E\boldsymbol{e}_x$. We assume that the electrons have reached a hydrodynamic regime characterizing a state of equilibrium of the system where the effects of collisions and forces are dominant, the EVDF has lost all memory of the initial state and the transport properties of the electrons do not change with time t and distance x any longer.

4.2.1. Multi-term method.
In the multi-term approach labeled BE MT in the following, we start from the time-dependent, spatially homogeneous version of the BE (9). We assume that the electrons have reached the hydrodynamic regime and their number density changes with time according to $n(t) \propto \exp(\nu_{eff} t)$. Then, $f(\boldsymbol{v}, t) = \hat{f}(\boldsymbol{v}) n(t)$ and $\partial_t f(\boldsymbol{v}, t)/n(t) = \nu_{eff} \hat{f}(\boldsymbol{v})$, so that the microscopic and macroscopic properties of the electrons result from the solution of the time-independent, spatially homogeneous BE for $\hat{f}(\boldsymbol{v})$. This distribution function is symmetric around the direction of the electric field, $\hat{f}(\boldsymbol{v}) = \hat{f}(v, v_x/v)$, where v_x is the x component of the velocity $\boldsymbol{v}$ with magnitude v. It can be expanded with respect to v_x/v in Legendre polynomials $P_k(v_x/v)$ with the integer $k = 0, \dots, l-1$. The substitution of this expansion into the BE finally leads to a hierarchy of partial differential equations for the expansion coefficients $f_k(v)$. The resulting system of equations with typically $l = 8$ expansion coefficients is solved using a generalized version of the solution technique given in [86]. Afterwards, we use the computed expansion coefficients $f_k(v)$ to determine e.g. the flux drift velocity $W^{\star}$, the flux transverse diffusion coefficient $D_T^{(0)}$ as well as the

ionization and attachment rate coefficients ν_i/N and ν_a/N. Explicit formulas of these transport parameters can be found in [45].

In order to determine transport coefficients at SST conditions in the multi-term approximation, we use the approach labeled BE SST in the present investigation. Here, we start from the time-independent, spatially 1D version of the BE (9). As soon as the electrons have reached their equilibrium state, their number density changes according to equation (7) and $f(x,\boldsymbol{v}) = n(x)\hat{f}(\boldsymbol{v})$. Consequently, $v_x \partial_x f(x,\boldsymbol{v})/n(x) = v_x \alpha_{\text{eff}} \hat{f}(\boldsymbol{v})$ and the transport coefficients at SST conditions can again be determined by solving a time-independent, spatially homogeneous BE for $\hat{f}(\boldsymbol{v})$. The rest of the procedure is similar to that for the BE MT approach. Notice that the resulting set of equations for the expansion coefficients differs from that of the BE MT approach as soon as ionization and attachment processes become relevant. The present multi-term approach BE SST provides fast access to the transport coefficients at SST conditions, but does not yield details about the spatial relaxation towards the equilibrium state itself. The effective ionization coefficient is given by $\alpha_{\text{eff}} = \nu_{\text{eff}}^{(\text{S})}/v^{(\text{S})}$ [45], where $\nu_{\text{eff}}^{(\text{S})}$ and $v^{(\text{S})}$ are the effective ionization frequency and average velocity at SST conditions, respectively.

4.2.2. Density gradient representation. This approach to describe the electron swarm at hydrodynamic conditions (labeled as BE DG below) is based on an expansion of the EVDF with respect to spatial gradients of the electron density n, of consecutive order. In this case, f depends on $(\boldsymbol{r},t)$ only via the density $n(\boldsymbol{r},t)$ and can be written as an expansion of the gradient operator ∇ according to

$$f(\boldsymbol{r},\boldsymbol{v},t) = \sum_{j=0}^{\infty} F^{(j)}(\boldsymbol{v}) \overset{j}{\odot} (-\nabla)^j n(\boldsymbol{r},t), \qquad (10)$$

where the expansion coefficients $F^{(j)}(\boldsymbol{v})$ are tensors of order j depending only on $\boldsymbol{v}$, and $\overset{j}{\odot}$ indicates a j-fold scalar product [71].

The expansion coefficients $F^{(j)}$ of order j are obtained from a hierarchy of equations for each component, all of which have the same structure and depend on the previous orders. In particular, to obtain the transport coefficients measured in TOF experiments, a total of five equations are required, namely for the expansion coefficients $F^{(0)}$, $F_{\text{L}}^{(1)}$, $F_{\text{T}}^{(1)}$, $F_{\text{LL}}^{(2)}$ and $F_{\text{TT}}^{(2)}$, while for the SST experiment one more equation for $F_{\text{L}}^{(\text{SST})}$ is required. In the present study, these equations are solved using a variant of the finite elements method given in [87] in a $(v, \cos\theta)$ grid.

From the above expansion coefficients we obtain two sets of transport coefficients: the *flux* coefficients, neglecting the contribution of non-conservative processes and equivalent to those obtained by the BE MT approach described in section 4.2.1, and the *bulk* coefficients including a contribution from ionization and attachment. The latter are, the *bulk* drift velocity,

$$W = W^{\star} + \int \nu_{\text{eff}}(v) F_x^{(1)}(\boldsymbol{v}) \mathrm{d}\boldsymbol{v} \qquad (11)$$

and the longitudinal and transverse components of the diffusion tensor,

$$D_{\text{L}} = \int v_x F_x^{(1)}(\boldsymbol{v}) \mathrm{d}\boldsymbol{v} + \int \nu_{\text{eff}}(v) F_{xx}^{(2)}(\boldsymbol{v}) \mathrm{d}\boldsymbol{v} \qquad (12)$$

$$D_{\text{T}} = \frac{1}{2} \left(\int v_{\text{T}} F_{\text{T}}^{(1)}(\boldsymbol{v}) \mathrm{d}\boldsymbol{v} + \int \nu_{\text{eff}}(v) F_{\text{TT}}^{(2)}(\boldsymbol{v}) \mathrm{d}\boldsymbol{v} \right) \qquad (13)$$

with v_{T} the transverse component of the velocity vector. Note that the first terms of the right-hand side of equations (11)–(13) are the *flux* component. Further details can be found in [45].

4.3. Monte Carlo simulation technique

In Monte Carlo simulations, we follow a large number of electrons (usually between 10^5 and 10^6, depending on simulation conditions) through CO gas under the influence of a uniform electric field. The Monte Carlo computer code is designed for simultaneous monitoring of a swarm of electrons under TOF and SST conditions. The electrons are released from the emitting boundary, which plays the role of the emitting cathode, with some initial velocity distribution and mean starting energy. The presence of electrons does not perturb the background CO molecules from the thermal equilibrium. The thermal motion of the background CO molecules is considered and implemented in the code using the procedure proposed by Ristivojević and Petrović [88]. Space charge effects and the screening of the externally applied electric field are neglected. Electrons acquire energy from the electric field and superelastic collisions, and dissipate this energy in elastic and inelastic collisions. It is presumed that collisions are binary and instantaneous. The scattering of electrons is isotropic for all kinds of collisions, regardless of the energy of the electrons. In case of electron attachment, the electrons are merely removed from the swarm. As for the ionization, the available energy after ionization was distributed assuming a uniform distribution indicating that all fractions of the available energy were equally probable between the primary and secondary electrons.

The position and velocity of each electron are updated after the time step, which is obtained as a fraction of the mean collision time. The exact time of collision is determined by a numeric solution of the equation for the probability of collision of the electron. The numerical solution of this equation involves the extensive use of random numbers. The type of collision is also determined using random numbers along with relative probabilities for individual collision processes and it determines the post-collision scattering parameters, including the speed of the electrons and the direction of motion. Details on the Monte Carlo method used in this work may be found in earlier publications [89, 90]. The Monte Carlo code was cross-checked against the numerical multi-term solutions of the BE for a range of model and real gases, and proved to be correct [90–92].

Under hydrodynamic conditions, the electron swarm transport coefficients are calculated after the relaxation of the swarm to the stationary state. The bulk transport coefficients,

which are universal transport quantities, can be calculated from the rate of change of the appropriate averages of the positions of the electrons, in configuration space [71, 78, 89]. The number changing reaction rate, which for electrons in CO is reduced to the effective ionization frequency, is defined by

$$\nu_{\text{eff}} = \frac{\mathrm{d}}{\mathrm{d}t} \left(\ln N_{\text{e}} \right), \tag{14}$$

where N_{e} is the total number of electrons at time t.

As the electric field is oriented along the x-axis, the explicit expressions

$$W = \frac{\mathrm{d}}{\mathrm{d}t} \left[\frac{\sum_{j=1}^{N_{\text{e}}} x_j(t)}{N_{\text{e}}} \right], \tag{15}$$

and

$$W^{\star} = \frac{1}{N_{\text{e}}} \sum_{j=1}^{N_{\text{e}}} \frac{\mathrm{d}x_j(t)}{\mathrm{d}t}, \tag{16}$$

are used for determining the bulk and flux drift speeds, respectively. The explicit expressions for the components of the diffusion tensor are

$$D_{\text{L}} = \frac{1}{2} \frac{\mathrm{d}}{\mathrm{d}t} \left[\langle x^2(t) \rangle - \langle x(t) \rangle^2 \right], \tag{17}$$

$$D_{\text{T}} = \frac{1}{4} \frac{\mathrm{d}}{\mathrm{d}t} \left[\langle y^2(t) + z^2(t) \rangle \right], \tag{18}$$

and

$$D_{\text{L}}^{\star} = \langle x v_x \rangle - \langle x \rangle \langle v_x \rangle, \tag{19}$$

$$D_{\text{T}}^{\star} = \frac{1}{2} \left(\langle y v_y \rangle + \langle z v_z \rangle \right) \tag{20}$$

where D_{L} and D_{T} are the bulk longitudinal and transverse diffusion coefficients, respectively, while $D_{\text{L}}^{\star}$ and $D_{\text{T}}^{\star}$ are the corresponding flux values.

Under non-hydrodynamic conditions in an idealized SST setup, the spatially resolved mean energy and average velocity are calculated via the so-called 'box-sampling' [55, 58, 62]. According to this method, the x-axis is divided into a large number of small boxes, each having a width of Δx and being infinite in the other spatial directions. The mean energy and/or average velocity may be defined in kth box, i.e. between $x_k - \Delta x/2$ and $x_k + \Delta x/2$ as follows:

$$\langle \xi \rangle_k = \left(\frac{1}{\Delta x} \int_{\boldsymbol{v}} \int\!\!\int_{x_k - \Delta x/2}^{x_k + \Delta x/2} f_{\text{SST}}(x, \boldsymbol{v}) \, \mathrm{d}x \mathrm{d}\boldsymbol{v} \right)^{-1} \frac{1}{\Delta x}$$

$$\times \int_{\boldsymbol{v}} \int_{x_k - \Delta x/2}^{x_k + \Delta x/2} \xi f_{\text{SST}}(x, \boldsymbol{v}) \, \mathrm{d}x \mathrm{d}\boldsymbol{v}$$

$$\approx \left(\sum_{j=1}^{N_{\text{e}}} \Delta t_j^k \right)^{-1} \sum_{j=1}^{N_{\text{e}}} \xi_j^k \Delta t_j^k, \tag{21}$$

where $f_{\text{SST}}(x, v)$ is the steady-state distribution function, ξ_k^j is the value of the quantity to be sampled when the jth electron is contained in the kth box, Δt_j^k is the residence time of the electron in that box, and N_{e} is the number of electrons that appear there. For more details on the Monte Carlo modeling of an idealized SST experiment, the reader is referred to [55, 58, 62, 63].

5. Results and discussion

The bulk drift velocity, bulk longitudinal diffusion coefficient and the ionization frequency of electrons in CO have been measured in the range of the reduced electric field from 2 Td to 1603 Td at a gas temperature T of 293 K. The pressure of the gas amounted between 11.8 Pa and 1010 Pa in the TOF measurements. In addition to the electron swarm transport coefficients resulting from the experiment via the fitting procedure described in section 2, we present corrected values of these measured data resulting from a procedure briefly described at the end of section 2 and detailed in [46].

After a discussion of previous measurements in section 5.1 and remarks about conditions considered in present kinetic studies based on the solution of the electron BE and MC simulations in section 5.2, we present our measured and kinetically calculated transport coefficients in section 5.3. Our measured results for each transport coefficient (uncorrected and corrected values) are available in the appendix. Furthermore, the present measured data as well as results of BE calculations and MC simulations are provided online at [93]. The measured data can also be found at [94]. Finally, we present and discuss our results under SST conditions in section 5.4.

5.1. Previous measurements

A limited number of experimental data sets on the drift and diffusion of electrons in CO exists in the literature. One of the earliest measurements of the drift velocity and transverse characteristic energy at room temperature, were those carried out by Skinker and White [95]. The drift velocity data of Pack *et al* [77] were obtained from measurements of electron transit times in a double-shutter drift tube between 77 K and 443 K. A similar experimental technique was used by Nakamura for measurements of the drift velocity and longitudinal diffusion coefficient over the range of E/N from 0.3 Td to 300 Td at room temperature [75]. Warren and Parker [96] employed the modified SST experiment with a segmented collector plate to measure the ratio of the transverse diffusion coefficient to mobility. Wagner *et al* [97] measured the drift velocity and longitudinal diffusion coefficient in a drift tube using the TOF principle. The full description of the design and operation of the drift tube used by Haddad and Milloy for measurements of the drift velocity [73] was given by Huxley and Crompton [70]. Using the Bradbury–Nielsen technique, which was described in great details by Huxley and Crompton, Petrović and Crompton measured the drift velocity [74]. Roznerski and Leja measured the drift velocity using the modified Bradbury–Nielsen TOF technique [98]. In this
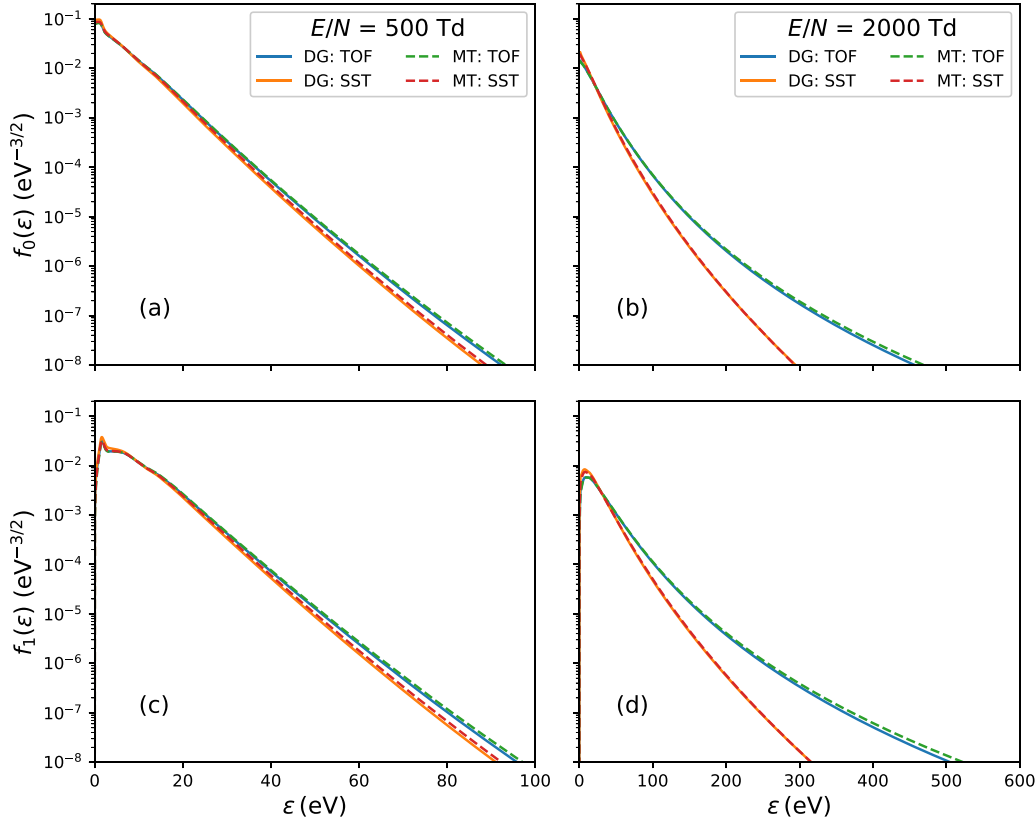
Figure 4. Isotropic (panels (a), (b)) and first anisotropic (c), (d) components of the EVDF for TOF or SST conditions, at two values of the reduced electric field ((a), (c): 500 Td; (b), (d): 2000 Td) computed with the BE MT and BE DG methods.

experiment, the standard Bradbury–Nielsen type of coplanar grid system [99–102] was replaced by a double grid system with the electrical shutters operated by an AC voltage applied between the adjacent grids. Measurements of the transverse characteristic energy by Petrović and Crompton were made by the Townsend–Huxley method using the apparatus with the fixed distance between the electrodes, and by the apparatus whose cathode-anode separation and anode configuration can be varied [74]. The experimental setup initially developed by Virr *et al* [103] was used by Saelee and Lucas [76] and by Lakshminarasimha *et al* [104] to measure the drift velocity and transverse characteristic energy.

The ionization coefficient was determined by measuring the pre-breakdown current in uniform fields at different pressures. In the same work of Bhalla and Craggs [105] first measurements of the rate coefficient for electron attachment were performed. The ionization coefficient was also measured by Davies and Williams [106] and by Parr and Moruzzi [107]. The data are taken from the LxCat database [108].

5.2. Simulation conditions

The kinetic studies of electron transport in CO, under both hydrodynamic and non-hydrodynamic conditions, cover a range of reduced electric field, E/N, between 0.01 Td and 2000 Td. The number of electrons in our Monte Carlo simulations under hydrodynamic conditions was varied between 2.5×10^5 and 1×10^6 depending on the applied E/N. Under

non-hydrodynamic conditions in an idealized SST setup, however, the number of electrons was varied between 1×10^5 and 5×10^5, depending on the distance between the electrodes and the applied E/N. The gas temperature was 293 K while the pressure was assumed to be 1 Torr. In section 5.4 we show the results of our study under hydrodynamic conditions, where the electron swarm transport coefficients are presented as a function of the reduced electric field E/N. In section 5.4, however, we present the results of our study under non-hydrodynamic conditions in an idealized SST setup, where the electron swarm transport properties are given as a function of E/N, while the spatial relaxation profiles of the mean energy and average velocity are presented as a function of the spatial position x. Due to the absence of three-body processes the Nx scaling applies here, where N is the gas number density. Under non-hydrodynamic conditions in an idealized SST setup, the electrons are released from the cathode assuming two different sets of initial conditions: (i) the beam initial velocity distribution with starting mean energies of 0.1 eV, 1 eV and 10 eV, and (ii) the Maxwell–Boltzmann initial velocity distribution with the same starting mean energies.

The electron distribution functions for TOF and SST conditions are practically the same at low E/N. As non-conservative processes become important, the distributions become increasingly different for TOF conditions with a small fraction of the electron swarm obtaining very high kinetic energies $\varepsilon = mv^2/2$. This can be seen in figure 4 where the first two expansion coefficients of the EVDF in Legendre polynomials,
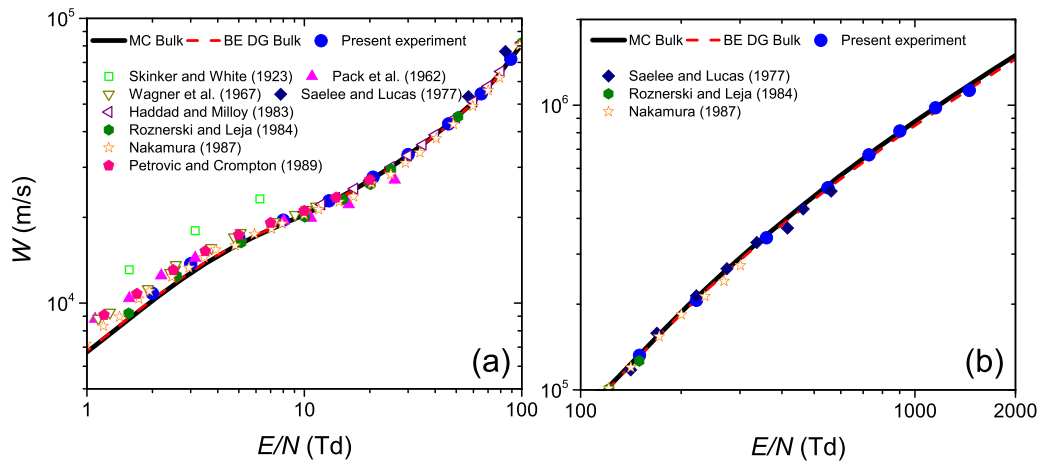
Figure 5. Comparison of the present measurements and kinetic calculations of the bulk drift velocity with other available experimental data. 'Present experiment' corresponds to the uncorrected experimental data. The corrected data are not presented here because of minor correction factors for the bulk drift velocity. Panel (a) shows a comparison over the range of E/N from 1 Td to 100 Td. Panel (b) shows a comparison over the range of E/N from 100 Td to 2000 Td.

computed in TOF or SST conditions are compared for two values of E/N, 500 Td when the two distributions are still very close and 2000 Td, the largest E/N considered. The results are obtained with both BE methods, with a very good agreement. A similar behavior was reported with pulsed discharges in air [66]. The figure allows a visual comparison of the amplitudes of the f_0 and f_1 components. We observe that for low kinetic electron energies $f_1 < f_0$ but as ε increases, the f_1 component becomes dominant, $f_1 \geqslant f_0$, showing that the high energy tail is pointed forward.

5.3. Electron swarm transport coefficients under hydrodynamic conditions

5.3.1. Drift velocity. In figure 5 we show the present experimental values of the drift velocity as a function of the reduced electric field E/N. They cover the E/N range 2 Td $\leqslant E/N \leqslant$ 1603 Td and are compared with our modeling results and other available experimental swarm data. Our modeling results include MC and BE DG calculations for the bulk drift velocity.

The agreement between our experimental results and those measured by Pack *et al* [77] is within 5% over the E/N range 2 Td $\leqslant E/N \leqslant$ 20 Td, while for smaller E/N values our results are lower by rather more than 10%. We also find fair agreement with the results of Wagner *et al* [97] between 3 Td and 12 Td, with the exception of a few experimental points below 3 Td where the scatter in their data is between 4% and 7%. The present experimental results are in good agreement with the measurements of Saelee and Lucas over the E/N range 100 Td $\leqslant E/N \leqslant$ 500 Td [76], where the maximal discrepancy between the two sets of data does not exceed 5%. For $E/N \leqslant$ 100 Td, however, the results of Saelee and Lucas are above the present experimental results by up to 10%. The results of Nakamura [75] are lower than the present experimental data by up to 5% between 2 Td and 20 Td and between 40 Td and 300 Td. Over the E/N range 20 Td $\leqslant E/N \leqslant$ 40 Td the agreement is slightly deteriorated and lies within 8%. The

agreement between the present experimental results and those of Roznerski and Leja [98] are within 4% between approximately 2 Td and 15 Td, and within 7% between 15 Td and 30 Td, while for the remaining higher values of E/N the agreement is better and lies within 1%. The present experimental results are in excellent agreement with the measurements of Haddad and Milloy (within 1%) [73], and with the data of Petrović and Crompton (within 1%) with the exception of a few points below 5 Td [74]. The largest discrepancy with respect to the present experimental results is found for the data of Skinker and White [95] by up to 25%, but one should bear in mind that this is one of the earliest measurements of the electron swarm data in CO with a large experimental error. Thus, we can conclude that, except for the data of Skinker and White [95], the present experimental results agree fairly well with all other available measurements. The discrepancy between the present experimental results and other available measurements may be attributed to a number of reasons, including the precision of the individual experimental setups, the presence of impurities in drift chambers, issues associated with the control of gas pressure in the chamber and current in the system of electrodes, thermal effects and diffusion cooling, and the interpretation of the drift velocity in various experimental setups when non-conservative processes are operative.

In figure 6 we show the comparison between the present experimental results and modeling results for the drift velocity. The present experimental data and the calculated bulk drift velocity generally agree very well over the entire range of E/N considered in this work. This indicates that the experimentally observed quantities in the scanning drift tube apparatus are the bulk transport coefficients. The differences between the bulk and flux values of the drift velocity become larger than 1% for $E/N \geqslant$ 130 Td, and continue to increase, reaching a value of approximately 35% in the limit of the largest E/N considered. This is a clear indication of the explicit effects of ionization processes on the transport coefficients. The production of new electrons by ionization shifts the swarm's
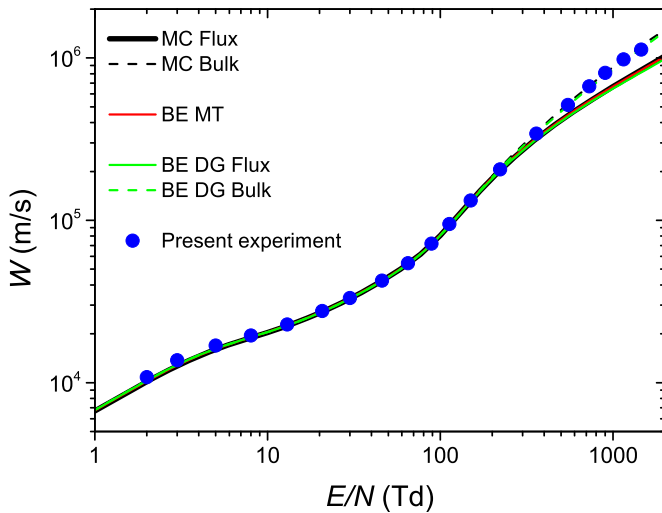
Figure 6. Comparison of the flux and bulk drift velocities, calculated using a Monte Carlo simulation technique and numerical solutions of the Boltzmann equation, and the present experimental values. 'Present experiment' corresponds to the uncorrected experimental data.
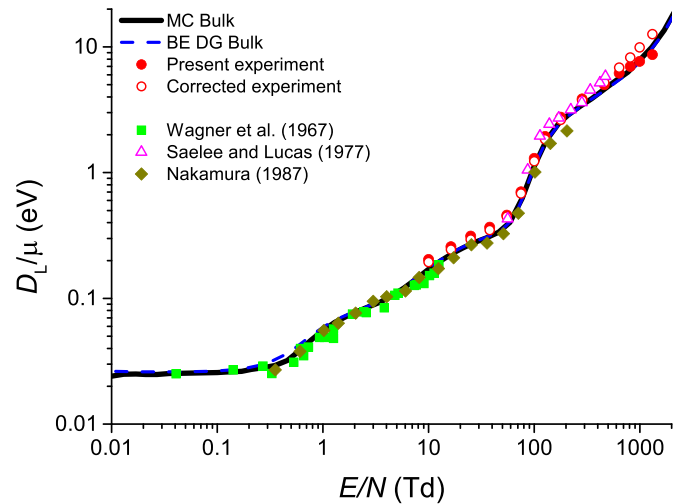

Figure 7. Comparison of the present measurements and kinetic calculations of the bulk longitudinal characteristic energy with other available experimental data. We present the uncorrected ('Present experiment') and corrected experimental data.

center of mass forward, which in turn enhances the measurable drift velocity. On the other hand, the explicit contribution of electron attachment to the measurable drift velocity was not observed.

For the flux drift velocity, the MC results are in excellent agreement with those obtained by the BE MT method over the entire range of E/N. We see that the calculations of the flux drift velocity using the BE DG method tend to lie a little below the remaining two sets of data. The discrepancy at approximately 150 Td is around 1% and continues to increase to 3.7% in the limit of the largest E/N considered in the present work. For the bulk drift velocity, our modeling results, including those obtained by the MC and BE DG methods, compare well with the present experimental results with the exception of a few points below 5 Td. As can be seen from figure 5, the disagreement between our MC and BE DG calculations, and measurements of Pack *et al* [77], Wagner *et al* [97] and Petrović and Crompton [74] is also evident for $E/N \leqslant 5$ Td. The experimental data of Roznerski and Leja [98], and Nakamura [75] are slightly more consistent with our modeling results, but still our results are below these measurements. In this low E/N range, the present experimental data tend to lie a little above the results of the present calculations, indicating the need for further refinement of the cross section for momentum transfer. At such low E/N, the exchange of momentum is controlled by rotational excitations. As recently discussed by Vialetto *et al* [32], one needs to implement the anisotropic scattering for the dipole-rotational collisions in Monte Carlo simulations and/or BE solutions to achieve better agreement between the measured and the calculated drift velocity. That remains the subject of future work. On the other hand, the agreement between the present experimental results and the calculated bulk drift velocity for $E/N \geqslant 5$ Td is within 3% with the exception at the higher end of the E/N range, where experimental data are up to 4% larger.

5.3.2. Diffusion coefficients. In figure 7 we show the variation of the longitudinal characteristic energy D_L/μ as a function of E/N. This property was not directly measured in the scanning drift tube apparatus, but was calculated using the experimental values of the longitudinal diffusion coefficient and drift velocity. The present experimental results include the two data sets, the directly measured data ('Present experiment'), and the data generated by the correction procedure ('Corrected experiment'). Since the behavior of the diffusion coefficients exhibits a certain sensitivity with respect to the non-uniform response of the detector in our measurements, the reference results are those produced by the correction procedure. As indicated in figure 7, the present modeling results include the MC and BE DG results for the bulk values of D_L/μ. Our measurements of the ND_L were performed for $E/N \geqslant 10$ Td since for lower values of E/N the accuracy of the determination of ND_L was remarkably decreased due to the worse signal to noise ratio.

There were a limited number of measurements on D_L/μ, and the three known to the authors are the measurements of Wagner *et al* [97], Saelee and Lucas [76], and Nakamura [75]. The TOF measurements of Wagner *et al* are given for lower values of E/N and outside the range in which our measurements were performed. Comparing experimental results of Wagner *et al* and our modeling results, we observe a fairly good agreement with MC results. This result can be understood by the fact that both the longitudinal diffusion coefficient D_L and the electron mobility μ are inversely proportional to the total momentum transfer cross section, making their ratio to become less sensitive to variations in this cross section [32]. The discrepancy between our experimental results and those of Saelee and Lucas ranges from about 1% at 60 Td to about 20% at 150 Td and within 7% over the E/N range 150 Td $\leqslant E/N \leqslant 500$ Td. The agreement between our experimental data and those published by Nakamura is within 10% for $E/N \leqslant 100$ Td, while for larger values of E/N the
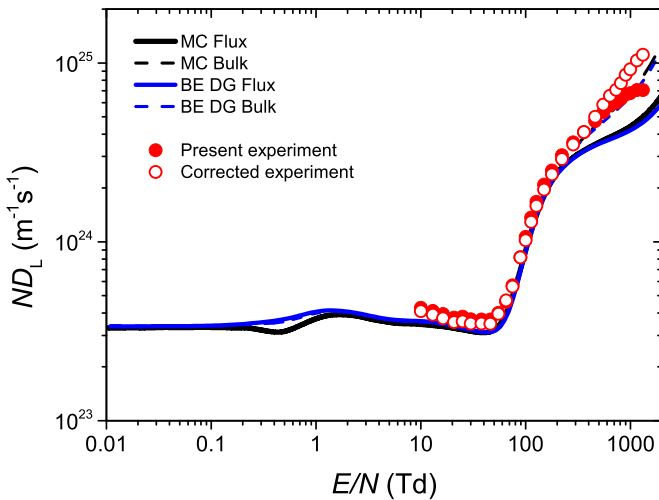
Figure 8. Comparison of the flux and bulk longitudinal diffusion coefficients, calculated using a Monte Carlo simulation technique and numerical solutions of the Boltzmann equation, and the present experimental values. The uncorrected ('Present experiment') and corrected experimental data are included.

agreement is deteriorated reaching the discrepancy of up to 30% at 240 Td. Comparing the present experimental and modeling results, the BE DG results agree better with the present measurements for $E/N \leqslant 60$ Td and for $E/N \geqslant 500$ Td, while MC results are in better agreement with the corresponding experimental data for the remaining intermediate values of E/N. It is important to note here that the application of the correction procedure to our experimental results leads to a much better agreement with both the previously measured data and the present modeling results, e.g. the calculated bulk values of D_L/μ.

The comparison between the present experimental and modeling results for the longitudinal diffusion coefficient is shown in figure 8. As for the drift velocity, the current experimental results agree much better with the bulk values of ND_L, indicating that the experimentally observable quantities are the bulk transport coefficients. In relation to the drift velocity, the longitudinal diffusion coefficient exhibits a slightly higher sensitivity with respect to the explicit effects of ionization. At 130 Td the differences between the flux and bulk values are approximately 1%, but with a further increase in E/N, the number of electrons increases due to ionization, which in turn enhances diffusion along the longitudinal direction. As a result, the difference between the flux and bulk values in the limit of the largest E/N is around 50%. On the other hand, the influence of electron attachment was insignificant for all E/N studied.

Comparing the drift velocity (figure 6) and the longitudinal diffusion coefficient (figure 8), the agreement between the corrected experimental results and modeling results is worse for the longitudinal diffusion coefficient. Between 10 Td and 60 Td, our measurements agree within 10% with the BE DG results, while over the intermediate E/N range 60 Td $\leqslant E/N \leqslant$ 350 Td, the agreement is better with the MC results and lies within 17%. For the remaining higher values of E/N, our

corrected experimental results are again in a better agreement with the BE DG results. Comparing MC and BE DG results, for $E/N \geqslant 50$ Td the agreement between the flux values is very good. The disagreement between the MC and BE DG results for the bulk longitudinal diffusion coefficient at higher E/N is within 5%. One of the striking results illustrated by figure 8 is a disagreement between the MC and BE DG results between approximately 0.1 Td and 40 Td. Despite several checks of the numerical procedures involved, we do not understand the origin and nature of the observed difference. This remains the subject of future work.

In figure 9 we show the variation of the transverse characteristic energy D_T/μ as a function of E/N. This property was not measured in the scanning drift tube apparatus and here we present our modeling results only. The modeling results include MC and BE DG results for the bulk and flux values of D_T/μ. The calculated bulk values of D_T/μ are in good agreement (within 3%) with the experimental data of Petrović and Crompton [74] between 50 Td and 120 Td, while at lower values of E/N the agreement is deteriorated reaching the discrepancy of 9% at 1 Td. The agreement between the present modeling results and those measured by Skinker and White [95] is relatively good (within 6%) for $E/N \geqslant 10$ Td, with the two exceptions at approximately 20 Td and 45 Td, where the agreement is slightly deteriorated and is within 8%. Over the E/N range $1 \leqslant E/N \leqslant 10$ Td our results are lower by up to 9%. There are larger discrepancies with the results of Warren and Parker [96] over the E/N range 8 Td $\leqslant E/N \leqslant 100$ Td. For $E/N \leqslant 8$ Td the discrepancy between our calculated bulk values of D_T/μ and those measured by Warren and Parker are huge as the measurements were performed at a gas temperature of 77 K, while our calculations were performed at 293 K. The agreement between our modeling results and those measured by Lakshminarasimha *et al* [104] is within 10% with the exceptions at the edges of the E/N range where the agreement is slightly deteriorated. It should be noted that over the E/N range 300 Td $\leqslant E/N \leqslant 1200$ Td the measurements of Lakshminarasimha *et al* are in better agreement with the BE DG results than with those obtained by applying the MC method. The comparison between our modeling results and the available experimental data reveals that our calculations are systematically below the experimental data. This clearly indicates the need for further refinement of the cross sections, especially the treatment of cross sections for dipole rotational excitations. The implementation of anisotropic scattering for dipole rotational excitations would improve the balance of momentum and energy within the lower E/N values.

The comparison between the individual methods for calculating the transverse diffusion coefficient is shown in figure 10. Comparing the transverse diffusion coefficient on one side, and the drift velocity and longitudinal diffusion coefficient on the other side, we observe that the transverse diffusion coefficient is somewhat less sensitive with respect to the explicit influence of ionization. We observe that the difference between the flux and bulk values of the transverse diffusion coefficient is not discernible below 130 Td. This difference increases with increasing E/N and reaches a value of about 35% at the largest E/N considered. As in the case of the drift
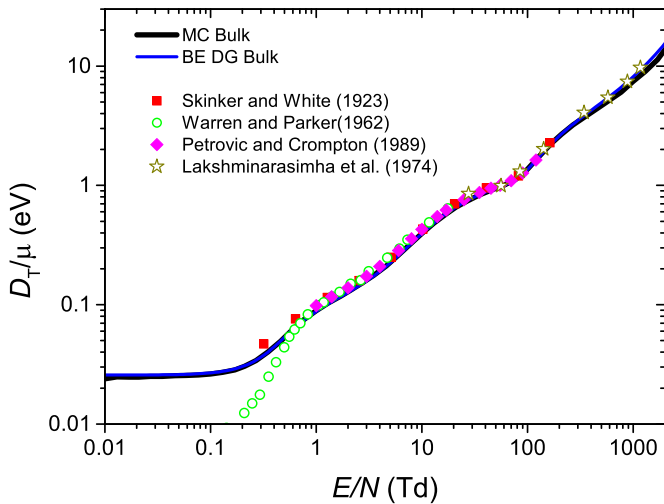
Figure 9. Comparison of the present kinetic calculations of the bulk transverse characteristic energy with other available experimental data.
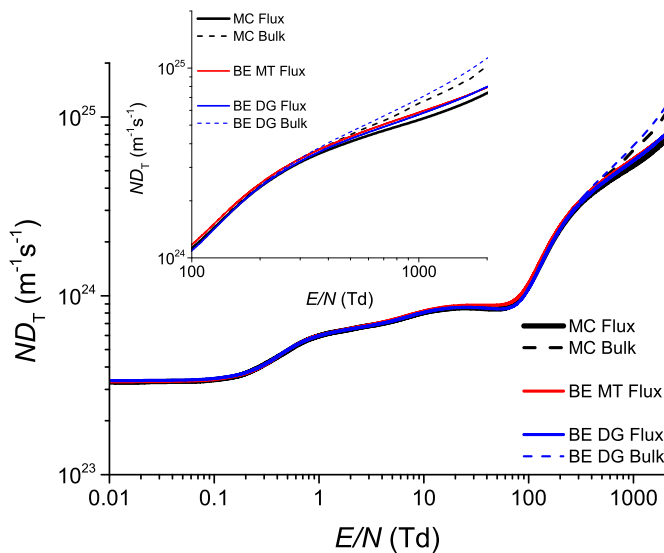

Figure 10. Comparison of the flux and bulk transverse diffusion coefficients, calculated using a Monte Carlo simulation technique and numerical solutions of the Boltzmann equation.

velocity and the longitudinal diffusion coefficient, it was found that the explicit influence of electron attachment on the transverse diffusion coefficient is negligible.

The overall agreement between individual modeling results for the transverse diffusion coefficient is good over the entire range of E/N. In particular, the MC and BE DG results for the flux values of ND_T agree within 2.5% up to approximately 500 Td. Within the same E/N range, the agreement between the MC and BE MT results is slightly lower and is less than 5%. While the MC results are slightly less consistent with the BE DG and BE MT results at higher values of E/N, the agreement between the BE DG and BE MT results is rather good.

5.3.3. Rate coefficients. Figure 11 displays the ionization rate coefficient $k_i = \nu_i/N$ and the attachment rate coefficient
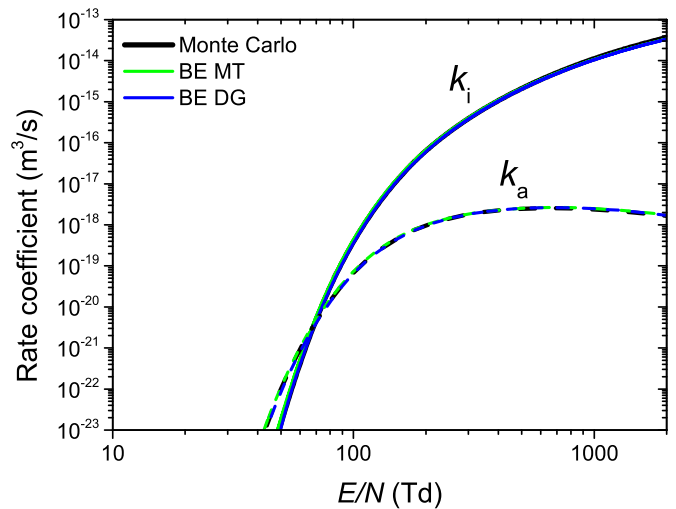

Figure 11. Comparison of the ionization and attachment rate coefficients, calculated using a Monte Carlo simulation technique and numerical solutions of the Boltzmann equation. The critical electric field is 69 Td.

$k_a = \nu_a/N$, where ν_i and ν_a denote the swarm average ionization and attachment frequencies, respectively. The MC results and those obtained by solving the BE agree very well. The critical electric field is defined as the E/N value for which the rate coefficient for ionization is equal to the rate coefficient for attachment. For electrons in CO, the critical electric field is approximately 69 Td, indicating that the production of free electrons by ionization dominates the loss of electrons by attachment for $E/N \geqslant 69$ Td. Although the critical electric field is 69 Td, the explicit contribution of ionization to the drift and diffusion of electrons in CO does not become apparent until 130 Td. This could be understood by considering the variation of the rate coefficients for the electron attachment and ionization over the E/N range 69 Td $\leqslant E/N \leqslant$ 130 Td. Within this E/N range, ionization and electron attachment are competitive processes with individual contributions that largely cancel each other out. Similar arguments can be used to understand the insignificant contribution of electron attachment to drift and diffusion for the E/N values that are lower than the critical electric field. In this case the transport modification by the explicit influence of electron attachment is prevented by the production of free electrons in ionizing collisions.

5.4. Electron swarm transport properties in an idealized SST setup

In this section we present results showing the spatially resolved electron swarm transport properties under non-hydrodynamic conditions in an idealized SST setup. Figure 12 displays the exponential growth of the electron number, in the region between the electrodes, as a function of E/N. The electrons are released from the cathode assuming an initial beam velocity distribution, with a starting energy of 1 eV. We observe that the growth rate of the number of electrons increases with increasing E/N, indicating that the electrons increasingly ionize CO molecules.
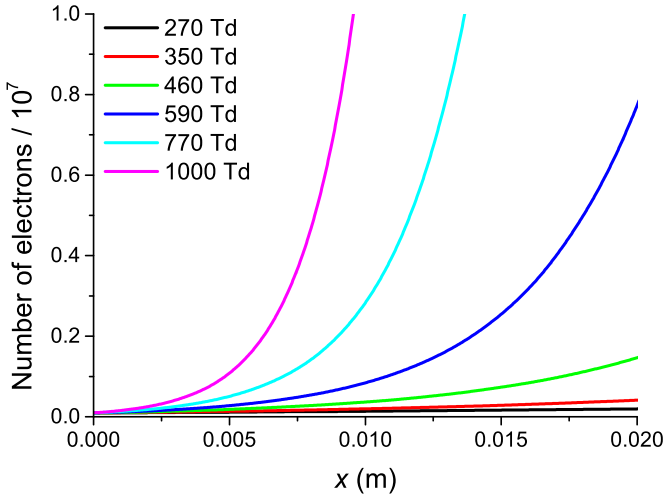
Figure 12. Exponential growth of the number of electrons in an idealized SST setup as a function of E/N.
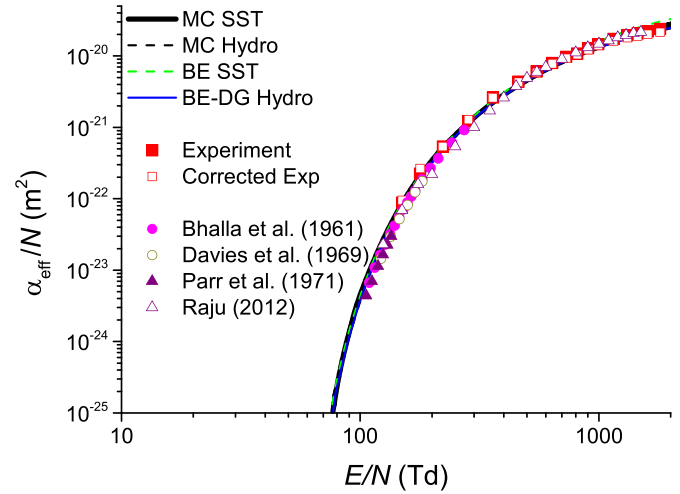

Figure 13. Comparison of the present measurements and kinetic calculations of the density-reduced effective Townsend ionization coefficient with other available experimental data. We present the uncorrected ('Present experiment') and corrected experimental data.

Using a Monte Carlo simulation technique, the density-reduced effective Townsend ionization coefficient α_{eff}/N in an idealized SST setup can be calculated in two ways. According to the first method, α_{eff}/N can be calculated by subtracting the density-reduced SST attachment coefficient η/N from the density-reduced SST ionization coefficient α/N at every spatial position x_k. In the present work, there are ten channels for ionizing CO molecule and just one channel for dissociative attachment. Therefore, the effective SST ionization coefficient was calculated from

$$\alpha_{\text{eff}} = \frac{\sum_{i=1}^{10} N_k^{\text{i}} - N_k^{\text{a}}}{\Delta x N_{\text{e}}(x_k)}, \tag{22}$$

where N_k^{i} denotes the number of ionizing collisions for every channel i, N_k^{a} is the number of collisions leading to dissociative attachment, Δx is the width of the spatial box, and $N_{\text{e}}(x_k)$ is the number of the resident electrons in the kth box. The second method is based on the fact that $\ln(N_{\text{e},2}/N_{\text{e},1})$ becomes linear as a function of x and α can be determined from the slope of the linear regression according to the equation:

$$\ln\left(\frac{N_{\text{e},2}}{N_{\text{e},1}}\right) = \alpha d, \tag{23}$$

where $N_{\text{e},2}$ and $N_{\text{e},1}$ are the number of electrons at the positions x_2 and x_1, respectively, and $d = x_2 - x_1$. The same procedure was used to determine the SST attachment coefficient η, where the slope is negative. The density-reduced Townsend ionization coefficient α/N was determined in low-current electrical discharges under SST conditions many times in the past using the similar approach: usually the dependence of $\ln(I/I_0)$ on the electrode gap distance is measured for various E/N values, where I is the discharge current and I_0 is the initial current at the cathode. Examples include the recent measurements of α/N in gas mixtures of He with N_2 [109], Ar with N_2 [110] as well as the recent measurements of α_{eff}/N in C5 perfluorinated ketone and its mixtures with air [111]. In the present modeling of an idealized SST setup, we have observed that

the agreement between the two methods is very good, except for the lowest values of E/N, where the number of ionizing collisions is significantly reduced. Under these conditions, electron-impact ionization collisions can be characterized as rare processes, which inevitably results in a deterioration of the statistics. In what follows, and in addition to the BE MT results, the MC results for α_{eff}/N were determined from the spatial profiles of the number of electrons.

In figure 13 we show the variation of the density-reduced effective Townsend ionization coefficient α_{eff}/N with E/N. The present experimental data for α_{eff}/N, are derived from the set of the measured data $\{\nu_{\text{eff}}/N, W, ND_{\text{L}}\}$ and equation (8). The results are compared with previous measurements and the present modeling results. The present modeling results include the MC and BE MT calculations under SST conditions (BE SST), while the MC and the BE DG results under hydrodynamic conditions (e.g. the MC Hydro and the BE DG Hydro) are derived from the set of the calculated transport coefficients $\{\nu_{\text{eff}}/N, W, ND_{\text{L}}\}$ and equation (8). The experimental data of Bhalla and Craggs [105] are given between approximately 105 Td and 273 Td, while the experimental data of Davies and Williams [106] and Parr and Moruzzi [107] are given over the E/N ranges, 122 Td $\leqslant E/N \leqslant$ 182 Td, and 106 Td $\leqslant E/N \leqslant$ 135 Td, respectively. The recommended data for α/N of Raju [112] extend over a much broader range of E/N, e.g. 125 Td $\leqslant E/N \leqslant$ 1500 Td. The present experimental values of α/N tend to lie a little above the previous measurements of Bhalla and Craggs [105] and Davies and Williams [106]. At lower values of E/N, the differences are up to 30%. However, as E/N increases, the difference between these two data sets is reduced. Comparing the present experimental results and those recommended by Raju [112], we observe the similar trend for $E/N < 400$ Td. For E/N higher than approximately 400 Td, the agreement between the present experimental data and Raju's recommended data is good and it is better than 10%. Comparing between our experimental and our experimental corrected data, we observe that Raju's
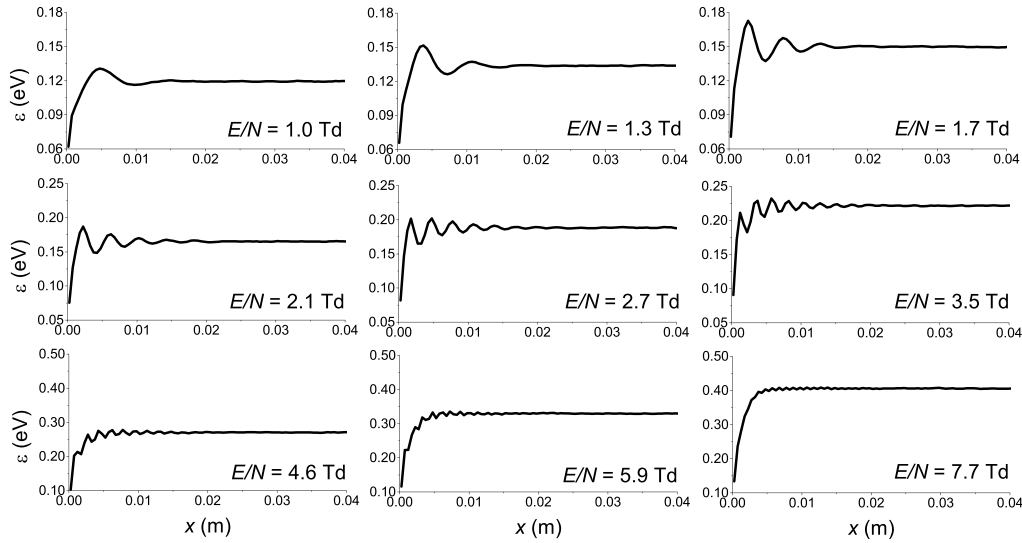
Figure 14. Spatial relaxation of the mean energy for electrons in CO over a range of E/N. Calculations are performed by a Monte Carlo simulation technique. The electrons are released from the cathode assuming an initial beam velocity distribution at an average starting energy of 0.1 eV.
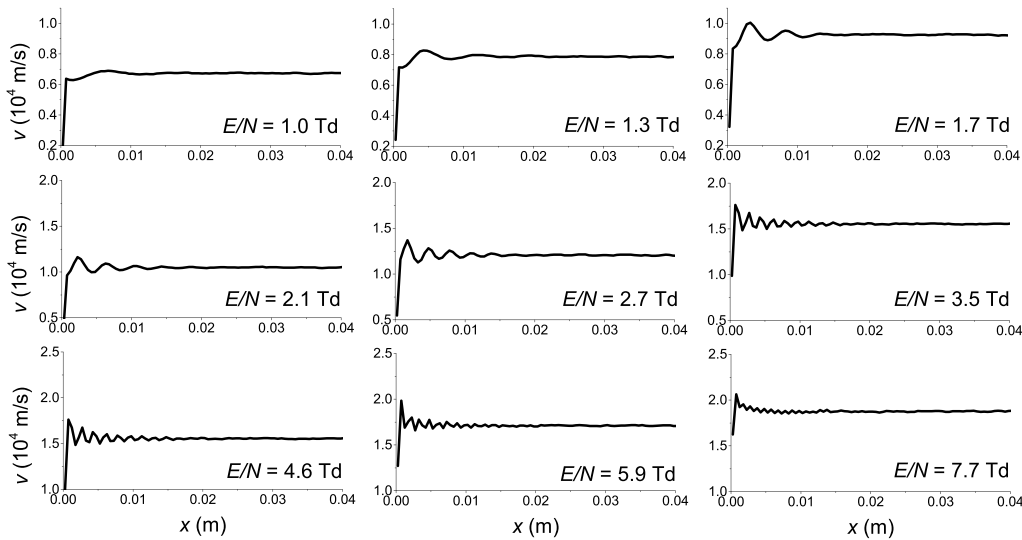

Figure 15. Spatial relaxation of the average velocity for electrons in CO over a range of E/N. Calculations are performed by a Monte Carlo simulation technique. The electrons are released from the cathode assuming an initial beam velocity distribution at an average starting energy of 0.1 eV.

recommended data agree much better with the uncorrected data.

For $E/N < 300$ Td the agreement between the present experimental and modeling results is very good and lies within 5%. For higher values of E/N the present experimental data agree very well with the modeling results (within 10%), particularly with the MC SST results. The agreement is slightly deteriorated at the three highest values of E/N (between 1300 Td and 1500 Td), between the corrected experimental data and modeling results. It should be noted that there is excellent agreement between the MC and BE DG results, when α_{eff}/N is calculated from the set of transport coefficients $\{\nu_{eff}/N, W, ND_L\}$ and equation (8).

Figures 14 and 15 display relaxation profiles of the mean energy and average velocity over the E/N range 1 Td $\leqslant E/N <$ 10 Td, as indicated on each panel. In both figures the electrons are released from the cathode assuming an initial beam velocity distribution, with a starting energy of 0.1 eV. The behavior of the mean energy and average velocity, and other transport properties is not considered in close vicinity of the anode. As electrodes were assumed to be perfectly absorbing in our simulations, the mean energy and average velocity sharply increase in the immediate vicinity of the anode. A similar behavior of spatially resolved mean energy in the immediate vicinity of a fully or partially absorbing anode was observed for model gases [113, 114], atomic gases [56–58, 62, 115, 116] and in O_2 at conditions typical of abnormal glow discharges [117].
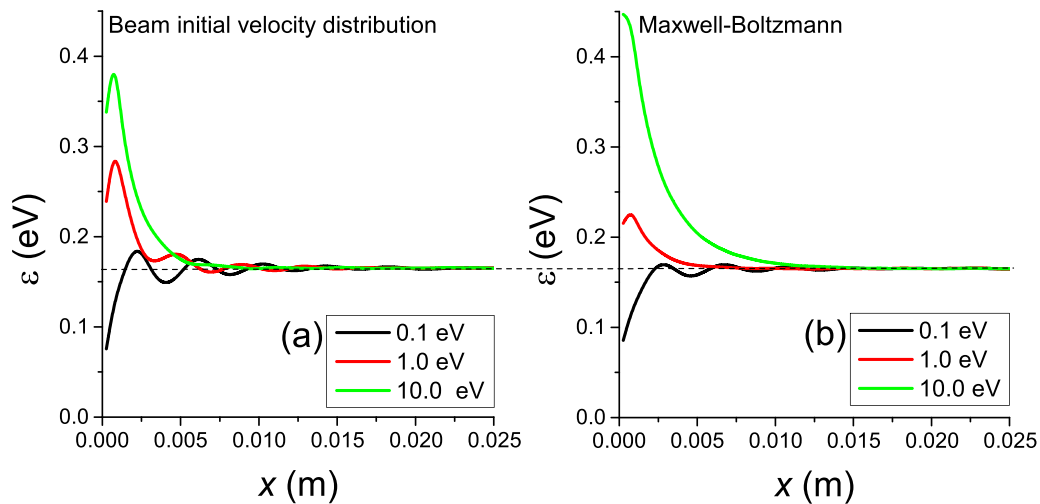
Figure 16. Spatial relaxation of the mean energy for electrons in CO at $E/N = 2.1$ Td. The calculations are for two different sets of initial conditions, including the initial beam velocity distribution (panel (a)) and a Maxwell initial velocity distribution (panel (b)), assuming starting mean energies of 0.1 eV, 1 eV and 10 eV, as indicated on the graph.

In figures 14 and 15, the oscillatory feature in the spatial relaxation profiles of mean energy and average velocity is clearly evident. However, for $E/N < 1$ Td or $E/N > 10$ Td, the oscillatory feature in the relaxation profiles of the mean energy and average velocity is firstly significantly reduced, and then completely removed. In addition, we have observed weak and irregular oscillations in the early stage of the spatial relaxation (i.e. in the close proximity to the fully absorbing cathode) of the mean energy and average velocity over the E/N range 130 Td $< E/N < 460$ Td.

The relaxation profiles of the mean energy and average velocity in CO are to a large extent consistent with earlier investigations on this topic for other molecular gases, including CH$_4$ [65], CF$_4$ [56] and synthetic air [66]. Firstly, we have observed a 'window' of E/N, where the spatially resolved transport properties exhibit oscillatory behavior as they relax towards the stationary state far downstream from the cathode. As shown in figure 16, this limited range of E/N, where the oscillatory feature in the spatial relaxation profiles takes place, depends on the initial conditions in the simulation. On the other hand, the spatially uniform values of mean energies are independent of the initial conditions. Secondly, the spatial relaxation characteristics, including the period and amplitude of the oscillations, and the equilibration length, are distinctively dependent on the applied E/N.

The spatial relaxation of the electrons and its characteristics, are controlled by the complex interplay between the collisional energy loss mechanisms. For $E/N < 1$ Td, the most frequent collisions between the electrons and CO molecule are elastic collisions, and inelastic collisions that lead to the rotational excitations. The elastic collisions produce monotonic relaxation to a spatially uniform state, by virtue of continuous energy losses in such processes. The presence of rotational excitations does not alter this physical picture as the mean energy of the electrons is much greater than the energy thresholds for the majority of rotational excitations. Thus, the oscillations in the spatial profiles of the mean energy and

average velocity over the E/N range of 1 Td $\leqslant E/N < 10$ Td, are induced by the 'discrete' energy losses associated with the vibrational excitations of CO molecule. However, as E/N increases, the collision frequency for the vibrational excitations of CO molecule increases. As a consequence, the elastic collisions in association with a large number of inelastic collisions that lead to the vibrational excitations, dampen the oscillatory behavior of the mean energy and average velocity. The period of oscillations is inversely proportional to the electric field strength, and an energy threshold that is a composite of several closely-lying vibrational excitations that control the relaxation process. Comparing to the spatial relaxation of the electrons in CH$_4$ [65], the spatial relaxation of the electrons in CO occurs much faster at lower values of E/N. This could be understood by considering the cross sections for electron scattering in CO, which favors faster relaxation. In addition, the spatial relaxation of electrons in CH$_4$ was considered using a significantly simplified set of cross sections, without ionization, electron attachment and rotational excitations. In other words, the set of cross sections used by Li *et al* [65] was not complete.

Figure 16 shows relaxation profiles of the mean energy for $E/N = 2.1$ Td, assuming two different sets of initial conditions, including the beam initial velocity distribution with mean starting energies of 0.1 eV, 1 eV and 10 eV (the first row), and a Maxwell velocity distribution with the same starting mean energies (the second row). In the first row of figure 16, where the beam initial velocity distribution is used for the initial conditions, we observe that increasing the mean starting energy from 0.1 eV to 1 eV reduces the equilibration length and makes the relaxation faster. The modulation amplitude and the period of oscillations are reduced with the exception of the first peak in the immediate vicinity of the cathode. Further enhancement of the mean starting energy to 10 eV modifies the spatial relaxation such that continuous energy loss mechanisms are dominant and relaxation is again monotonic. When a Maxwell velocity distribution is used for the initial electrons

at the cathode (second row of figure 16), we observe similar, but not identical effects. In this case, when the mean starting energy is increased from 0.1 eV to 1 eV, the oscillatory feature in the profile of the mean energy disappears and the relaxation is monotonic. This could be explained by considering the fact that for Maxwell's velocity distribution, the electrons can have a wider range of velocities, so the balance between energy gains from the field and losses in numerous binary collisions with CO molecules is achieved faster. The same arguments may be used to understand the differences between the spatial profiles for the two sets of initial conditions when the mean starting energy is 0.1 eV.

6. Concluding remarks

We have studied the electron transport in CO experimentally using a scanning drift-tube apparatus as well as computationally by solving the electron BE employing different approaches and via Monte Carlo simulations under hydrodynamic TOF conditions. In addition numerical studies have been carried out under non-hydrodynamic conditions in an idealized SST setup.

The scanning drift-tube apparatus was operated under TOF conditions allowing us to record 'swarm maps' initiated by short UV laser pulses. The recorded maps of the swarms allowed to extract the transport coefficients of the electrons by fitting the current signals. Since the current signals are directly related to the electron density, the extraction of the bulk drift velocity, the bulk longitudinal diffusion coefficient and the effective ionization frequency was performed using the solution of the diffusion equation. Using the measured electron swarm transport coefficients under TOF conditions, we derived the density-reduced effective SST ionization coefficient. The extracted and derived electron swarm transport coefficients were compared with previous measurements and modeling results over the broad range of E/N from 2 Td to 1603 Td. We found generally good agreement between the present experimental and modeling results with those originating from previous measurements. The largest deviations between the present measurements of the drift velocity and the corresponding results of modeling were observed in the limit of lower values of E/N, which indicates the possible need for further refinement of the electron collision cross sections for CO. The much larger deviation was observed between the experimental values and the modeling results for the longitudinal diffusion coefficient, which could be expected given the sensitivity of the detector system to the electron energy distribution, on the one hand, and to the sensitivity of this transport quantity to the energy dependence of the cross sections, on the other hand, in the context of modeling studies. Nevertheless, it can be concluded that the most recent set of cross sections for electron scattering in CO proposed by Biagi in Magboltz v11.11, although very complex and with a large number of individual cross sections for inelastic collisions, provides a good agreement between the experimental values of transport coefficients and the modeling results for electrons in CO gas. In other words, the present work indicates that the most recent

cross-sections set for electron scattering in CO from Magboltz v11.11, is *complete* because it includes all the necessary processes, allowing the calculation of transport coefficients and the velocity distribution function of the electrons using kinetic modeling. Likewise, the same set of cross sections may be regarded as *consistent* since it is able to reproduce the measured values of electron swarm transport coefficients within an order of 10% (with a few exceptions for ND_L), when used as an input in Monte Carlo simulations and for solving the electron BE.

We have also studied the electron transport and the spatial relaxation of the electrons under non-hydrodynamic conditions in an idealized SST setup. In Monte Carlo simulations, the electrons were released from the emitting boundary, which plays a role of the cathode, with a certain velocity distribution, and the evolution of the electrons was followed as a function of spatial position. Following previous works on this topic, it was shown that the spatial relaxation characteristics of transport quantities, including the equilibration length, the modulation amplitude and the period of oscillations, were guided and controlled by an interplay between the collisional energy loss mechanisms. We have found a 'window' of E/N between approximately 1 Td and 10 Td, for which all transport quantities exhibit oscillatory behavior as they relax to the spatially uniform state far downstream from the cathode. Comparing beam initial velocity distribution and the Maxwell–Boltzmann initial velocity distribution of the electrons, it was observed that the beam initial velocity distribution affects more spatial profiles of the mean energy and average velocity. For beam initial velocity distribution the spatial relaxation was slower, the oscillatory feature in the spatial profiles was more pronounced and the transition from an oscillatory to a monotonic relaxation occurred at higher values of E/N. Finally, the density-reduced effective Townsend ionization coefficient was evaluated directly from the spatial profiles of the number of electrons in an idealized SST setup and compared with the value derived using the hydrodynamic results of the effective ionization rate coefficient, the bulk drift velocity and the bulk longitudinal diffusion coefficient. We found a fairly good agreement between the two sets of data with the two exceptions at the highest E/N.

This study forms a sound basis for future swarm studies on electron transport in CO. The present experimental and modeling results offer a significant potential for future adjustments and improvements of the existing cross sections for electron scattering in CO. Likewise, the set of cross sections used in the present work and the associated swarm data might be gainfully applied to the modeling of electron transport in radio-frequency electric and magnetic fields. Other examples include the kinetic and fluid-equation based modeling of pulsed nanosecond discharges and a variety of plasma sources for the activation of CO_2 molecules.

Data availability statement

Acknowledgments

Appendix

Table 1 presents both the raw experimental data and their corrected counterparts for the bulk drift velocity and bulk longitudinal diffusion coefficient, as well as for the density-reduced effective Townsend ionization coefficient of electrons in CO gas. For the details of the correction procedure, see the text.

Table 1. Measured (*exptl.*) and corrected (*corr.*) data for different values of the reduced electric field.

| | W | | ND_L | | α_{eff}/N | |
| | $(10^4\,\mathrm{ms}^{-1})$ | | $(10^{23}\,\mathrm{m}^{-1}\,\mathrm{s}^{-1})$ | | $(10^{-22}\,\mathrm{m}^2)$ | |
E/N (Td)	*exptl.*	*corr.*	*exptl.*	*corr.*	*exptl.*	*corr.*
2	1.08	0.82				
3	1.37	1.19				
4	1.56	1.42				
5	1.69	1.61				
6	1.83	1.78				
8	1.95	1.97				
10	2.09	2.13	4.27	4.35		
13	2.29	2.36	4.11	4.19		
16.3	2.50	2.58	3.95	3.98		
20.7	2.77	2.85	3.77	3.75		
25	3.05	3.14	3.81	3.77		
30	3.33	3.42	3.69	3.61		
38	3.78	3.88	3.68	3.59		
46	4.26	4.34	3.68	3.51		
55	4.80	4.91	4.01	3.97		
65	5.44	5.55	4.62	4.58		
75	6.08	6.17	5.71	5.44		
89	7.19	7.27	8.22	7.57		
100	8.21	8.20	10.66	9.60		
113	9.49	9.44	13.67	12.02		
127	10.93	10.86	16.74	14.94		
150	13.23	13.09	20.87	18.78	0.88	1.27
178	16.12	15.93	25.05	23.16	2.25	2.17
222	20.64	20.43	30.49	29.04	5.39	5.53
284	26.47	26.33	35.97	35.87	12.18	12.01
360	34.24	34.35	41.04	42.91	26.31	25.90
460	43.51	44.09	47.31	53.07	43.90	40.68
549	51.33	52.77	53.02	62.41	60.91	56.62
637	59.40	61.39	57.70	70.46	79.86	71.49
729	66.93	70.18	59.89	76.43	97.40	87.07
811	73.08	77.30	63.07	82.43	108.51	97.17
902	81.11	86.59	66.59	89.46	129.14	112.32
995	87.62	94.78	67.79	93.56	146.93	127.87
1153	97.99	106.74	70.51	100.79	173.11	143.50
1314	106.47	117.96	70.55	103.99	195.21	158.58
1455	112.80	125.83	71.68	106.76	206.26	168.33
1603	116.20	131.67	67.36	101.93	220.71	178.27

ORCID iDs

S Dujko https://orcid.org/0000-0002-4544-9106
D Bošnjaković https://orcid.org/0000-0002-2725-5287
M Vass https://orcid.org/0000-0001-9865-4982
P Hartmann https://orcid.org/0000-0003-3572-1310
N R Pinhão https://orcid.org/0000-0002-4185-2619
D Loffhagen https://orcid.org/0000-0002-3798-0773
Z Donkó https://orcid.org/0000-0003-1369-6150

References

[1] Campbell L and Brunger M J 2008 *PMC Phys.* B **1** 1
[2] Campbell L, Allan M and Brunger M J 2011 *J. Geophys. Res.* **116** A09321
[3] Köhn C, Chanrion O, Enghoff M B and Dujko S 2022 *Geophys. Res. Lett.* **49** e2021GL097504
[4] Fleury B, Carrasco N, Gautier T, Mahjoub A, He J, Szopa C, Hadamcik E, Buch A and Cernogora G 2014 *Icarus* **238** 221
[5] Hörst S M and Tolbert M A 2014 *Astrophys. J.* **753** 53
[6] Moran S E, Hörst S M, He C, Radke M J, Sebree J A, Izenberg N R, Vuitton V, Flandinet L, Orthous-Daunay F R and Wolters C 2021 *J. Geophys. Res. Planets* **127** e2021JE006984
[7] Weaver H A, Feldman P D, McPhate J B, A'Hearn M F, Arpigny C and Smith T E 1994 *Astrophys. J.* **422** 374
[8] Campbell L and Brunger M J 2009 *Geophys. Res. Lett.* **36** L03101
[9] Konatham S, Torres J M and Zorzano M P 2020 *Proc. R. Soc.* A **476** 202001482
[10] Encrenaz T 2022 *Icarus* **376** 114885
[11] Ruffle D P, Rae J G L, Pilling M J, Hartquist T W and Herbst E 2002 *Astron. Astrophys.* **381** L13
[12] Itikawa Y 2015 *J. Phys. Chem. Ref. Data* **44** 013105
[13] Kwon S R, Kim K N, Nam C W and Woo S I 1995 *J. Vac. Sci. Technol.* B **13** 914
[14] Omori N, Matsuo H, Watanabe S and Puschmann M 1996 *Surf. Sci.* **352–354** 988
[15] Carbone E and Douat C 2018 *Plasma Med.* **8** 93
[16] Ionin A A 2006 Electric discharge CO lasers *Gas Lasers* ed M Endo and R F Walter (Boca Raton, FL: CRC Press) p 201
[17] Grigorian G M and Kochetov I V 2008 *Quantum Electron.* **38** 222
[18] Nighan W L 1970 *Phys. Rev.* A **2** 1989
[19] Nighan W L 1977 *Phys. Rev.* A **16** 1209
[20] Yardley J T 1971 *Appl. Opt.* **10** 1760
[21] Janeco A, Pinhão N R and Guerra V 2015 *J. Phys. Chem.* C **119** 109–20
[22] Ozkan A, Dufour T, Arnoult G, De Keyzer P, Bogaerts A and Reniers F 2015 *J. CO$_2$ Util.* **9** 74–81
[23] Cimerman R, Račková D and Hensel K 2018 *J. Phys. D: Appl. Phys.* **51** 274003
[24] Ristić M M, Aoneas M M, Vojnović M M, Galijaš S M D and Poparić G 2018 *Plasma Chem. Plasma Process.* **38** 903
[25] Guerra V, Silva T, Ogloblina P, Grofulović M, Terraz L, Silva M, Pintassilgo C D, Alves L L and Guaitella O 2017 *Plasma Sources Sci. Technol.* **26** 11LT01
[26] Guerra V, Silva T and Guaitella O 2018 *Europhys. News* **49** 15
[27] Pietanza L D, Colonna G and Capitelli M 2017 *Plasma Sources Sci. Technol.* **26** 125007
[28] Bogaerts A, Kozák T, van Laer K and Snoeckx R 2015 *Faraday Discuss.* **183** 217
[29] Trajmar S, Register D F and Chutjian A 1983 *Phys. Rep.* **97** 219
[30] Brunger M J and Buckman S J 2002 *Phys. Rep.* **357** 215
[31] Anzai K *et al* 2012 *Eur. Phys. J.* D **66** 36
[32] Vialetto L, Moussa A B, van Dijk J, Longo S, Diomede P, Guerra V and Alves L L 2021 *Plasma Sources Sci. Technol.* **29** 075001
[33] Hake R D Jr and Phelps A V 1967 *Phys. Rev.* **158** 70
[34] Land J E 1978 *J. Appl. Phys.* **49** 5716
[35] 2022 Phelps database (available at: www.lxcat.net) (Accessed 20 January 2022)
[36] Poparić G B, Belić D S and Vićić M D 2006 *Phys. Rev.* A **73** 062713
[37] Vojnović M, Popović M, Ristić M M, Vićić M D and Poparić G B 2013 *Chem. Phys.* **423** 1
[38] Aoneas M M, Vojnović M M, Ristić M M, Vićić M D and Poparić G B 2017 *Phys. Plasmas* **24** 023502

[39] Biagi S Unpublished cross-section set (available at http://magboltz.web.cern.ch/magboltz/)

[40] Ogloblina P, Tejero-del-Caz A, Guerra V and Alves L L 2020 *Plasma Sources Sci. Technol.* **30** 075001

[41] Alves L 2014 *J. Phys.: Conf. Ser.* **565** 012007

[42] Tejero-del-Caz A, Guerra V, Goncalves D, da Silva M L, Marques L, Pinhão N, Pintassilgo C D and Alves L L 2019 *Plasma Sources Sci. Technol.* **28** 043001

[43] Korolov I, Vass M, Bastykova N K and Donkó Z 2016 *Rev. Sci. Instrum.* **87** 063102

[44] Korolov I, Vass M and Donkó Z 2016 *J. Phys. D: Appl. Phys.* **49** 415203

[45] Vass M, Korolov I, Loffhagen D, Pinhão N and Donkó Z 2017 *Plasma Sources Sci. Technol.* **26** 065007

[46] Pinhão N, Loffhagen D, Vass M, Hartmann P, Korolov I, Bošnjaković D, Dujko S and Donkó Z 2020 *Plasma Sources Sci. Technol.* **29** 045009

[47] Vass M, Egüz E, Chachereau A, Hartmann P, Korolov I, Hösl A, Bošnjaković D, Dujko S, Donkó Z and Franck C 2020 *J. Phys. D: Appl. Phys.* **54** 035202

[48] Donkó Z, Hartmann P, Korolov I, Jeges V, Bošnjaković D and Dujko S 2019 *Plasma Sources Sci. Technol.* **28** 095007

[49] Okhrimovskyy A, Bogaerts A and Gijbels R 2002 *Phys. Rev.* E **65** 037402

[50] Sigeneger F and Winkler R 1997 *Plasma Chem. Plasma Process.* **17** 281–303

[51] Robson R E, Li B and White R D 2000 *J. Phys. B: At. Mol. Opt. Phys.* **33** 507

[52] Winkler R, Loffhagen D and Sigeneger F 2002 *Appl. Surf. Sci.* **192** 50–71

[53] Sigeneger F, Dyatko N A and Winkler R 2003 *Plasma Chem. Plasma Process.* **23** 103–16

[54] Loffhagen D 2005 *Plasma Chem. Plasma Process.* **25** 519–38

[55] Dujko S, White R D and Petrović Z L 2008 *J. Phys. D: Appl. Phys.* **41** 245205

[56] Dujko S, White R D, Petrović Z L and Robson R E 2011 *Plasma Sources Sci. Technol.* **20** 024013

[57] White R D, Robson R E, Nicoletopoulos P and Dujko S 2012 *Eur. Phys. J.* D **66** 117

[58] Dujko S, White R D, Raspopović Z M and Petrović Z L 2012 *Nucl. Instrum. Methods Phys. Res.* B **279** 84

[59] Loffhagen D 2016 Multi-term and non-local electron Boltzmann equation *Plasma Modeling: Methods and Applications* ed G Colonna and A D'Angelo (Bristol: IOP Publishing) pp 3-1–30

[60] Magyar P, Korolov I and Donkó Z 2012 *Phys. Rev. E* **85** 056409

[61] Dyatko N A, Kochetov I V and Ochkin V N 2020 *Plasma Sources Sci. Technol.* **29** 125007

[62] Dujko S *et al* 2021 *Plasma Sources Sci. Technol.* **30** 115019

[63] Dyatko N A, Kochetov I V and Ochkin V N 2021 *Phys. Rev.* E **104** 065204

[64] Sigeneger F and Winkler R 1997 *Plasma Chem. Plasma Process.* **17** 1–19

[65] Li B, White R D and Robson R E 2002 *J. Phys. D: Appl. Phys.* **35** 2914

[66] Hoder T, Loffhagen D, Voráč J, Becker M M and Brandenburg R 2016 *Plasma Sources Sci. Technol.* **25** 025017

[67] Ramo S 1939 *Proc. IRE* **27** 584

[68] Shockley W 1938 *J. Appl. Phys.* **9** 635

[69] Sirkis M D and Holonyak N Jr 1966 *Am. J. Phys.* **34** 943

[70] Huxley L G H and Crompton R W 1974 *The Diffusion and Drift of Electrons in Gases* (New York: Wiley-Interscience)

[71] Kumar K, Skullerud H R and Robson R E 1980 *Aust. J. Phys.* **33** 343

[72] Allan M 2010 *Phys. Rev.* E **81** 042706

[73] Haddad G N and Milloy H B 1983 *Aust. J. Phys.* **36** 473

[74] Petrović Z L and Crompton R W 1989 *Aust. J. Phys.* **42** 609

[75] Nakamura Y 1987 *J. Phys. D: Appl. Phys.* **20** 933

[76] Saelee H T and Lucas J 1977 *J. Phys. D: Appl. Phys.* **10** 343

[77] Pack J L, Voshall R E and Phelps A V 1962 *Phys. Rev.* **127** 2084

[78] Robson R E 1991 *Aust. J. Phys.* **44** 685

[79] Simonović I, Bošnjaković D, Petrović Z L, Stokes P, White R D and Dujko S 2020 *Phys. Rev.* E **101** 023203

[80] Simonović I, Bošnjaković D, Petrović Z L, White R D and Dujko S 2022 *Plasma Sources Sci. Technol.* **31** 015003

[81] Petrović Z L, Dujko S, Marić D, Malović G, Nikitović Ž, Šašić O, Jovanović J, Stojanović V and Radmilović-Radjenović M 2009 *J. Phys. D: Appl. Phys.* **42** 194002

[82] Thomas W R L 1969 *J. Phys. B: At. Mol. Phys.* **2** 551

[83] Blevin H A and Fletcher J 1984 *Aust. J. Phys.* **37** 593

[84] Robson R E, White R D and Ness K F 2011 *J. Chem. Phys.* **134** 064319

[85] Margenau H 1948 *Phys. Rev.* **73** 297–308

[86] Leyh H, Loffhagen D and Winkler R 1998 *Comput. Phys. Commun.* **113** 33–48

[87] Segur P, Bordage M C, Balaguer J P and Yousfi M 1983 *J. Comput. Phys.* **50** 116

[88] Ristivojević Z and Petrović Z L 2012 *Plasma Sources Sci. Technol.* **21** 035001

[89] Dujko S, Raspopović Z M and Petrović Z L 2005 *J. Phys. D: Appl. Phys.* **38** 2952

[90] Dujko S, White R D, Petrović Z L and Robson R E 2010 *Phys. Rev.* E **81** 046403

[91] Raspopović Z M, Sakadzic S, Bzenić S and Petrović Z L 1999 *IEEE Trans. Plasma Sci.* **27** 1241

[92] Petrović Z L, Raspopović Z M, Dujko S and Makabe T 2002 *Appl. Surf. Sci.* **192** 1

[93] Loffhagen D, Dujko S, Bošnjaković D, Vass M, Hartmann P, Korolov I, Pinhão N R and Donkó Z 2023 Electron swarm transport coefficients in CO—measurements and kinetic studies INPTDAT (https://doi.org/10.34711/inptdat.548)

[94] Budapest Drift Tube Database (available at: www.lxcat.net)

[95] Skinker M F and White J V 1923 *Phil. Mag.* **46** 630

[96] Warren R W and Parker J H 1962 *Phys. Rev.* **128** 2661

[97] Wagner E B, Davis F J and Hurst G S 1967 *J. Chem. Phys.* **47** 3138

[98] Roznerski W and Leja K 1984 *J. Phys. D: Appl. Phys.* **17** 279

[99] Bradbury N E and Nielsen R A 1936 *Phys. Rev.* **49** 388

[100] Crompton R W, Elford M T and Gascoigne J 1965 *Aust. J. Phys.* **18** 409

[101] Crompton R W, Elford M T and Jory R L 1967 *Aust. J. Phys.* **20** 369

[102] Blevin H A and Hasan M Z 1967 *Aust. J. Phys.* **20** 735

[103] Virr L E, Lucas J and Kontoleon N 1972 *J. Phys. D: Appl. Phys.* **5** 542

[104] Lakshminarasimha C S, Lucas J and Kontoleon N 1974 *J. Phys. D: Appl. Phys.* **7** 2545

[105] Bhalla M S and Craggs J D 1961 *Proc. Phys. Soc.* **78** 438

[106] Davies G H L and Williams A W 1969 *Contributed Papers 9th Int. Conf. on Phenomena in Ionized Gases (Bucharest, 1–6 September 1969)* (Bucharest: Academy of the Socialist Republic of Romania) p 46

[107] Parr J E and Moruzzi J L 1971 *Proc. 10th Int. Conf. on Phenomena in Ionized Gases* p 8

[108] Pitchford L C *et al* 2017 *Plasma Process. Polym.* **14** 1600098

[109] Talviste R, Paris P, Raud J, Plank T and Jõgi I 2021 *J. Phys. D: Appl. Phys.* **54** 325202

[110] Talviste R, Paris P, Raud J, Plank T, Erme K and Jõgi I 2021 *J. Phys. D: Appl. Phys.* **54** 465201

[111] Aints M, Jõgi I, Laan M, Paris P and Raud J 2018 *J. Phys. D: Appl. Phys.* **51** 135205

[112] Raju G G 2012 *Gaseous Electronics: Tables, Atoms and Molecules* (Boca Raton, FL: CRC Press)

[113] Lowke J J, Parker J H and Hall C A 1977 *Phys. Rev.* A **15** 1237–45

[114] Braglia G L and Lowke J J 1979 *J. Phys. D: Appl. Phys.* **12** 1831–8

[115] Petrova T and Petrov G M 2000 *Phys. Scr.* **61** 102–11

[116] Loffhagen D, Sigeneger F and Winkler R 2002 *J. Phys. D: Appl. Phys.* **35** 1768–76

[117] Grubert G K and Loffhagen D 2014 *J. Phys. D: Appl. Phys.* **47** 025204